





Article

The trace-element compositions of amphibole, magnetite and ilmenite as potential exploration guides to metamorphosed Proterozoic Cu–Zn±Pb±Au±Ag volcanogenic massive sulfide deposits in Colorado, USA

Paul G. Spry¹ , Edward H. Berke¹, Dan Layton-Matthews², Alexandre Voinot² , Adriana Heimann³, Graham S. Teale⁴ and Anette von der Handt⁵

¹Department of Geological and Atmospheric Sciences, Iowa State University, Ames, Iowa, USA; ²Department of Geological Sciences and Geological Engineering, Queen's University, 36 Union Street, Kingston, Ontario, Canada; ³Department of Geological Sciences, 101 Graham Building, East Carolina University, East 5th Street, Greenville, North Carolina, USA; ⁴Teale & Associates Pty Ltd, PO Box 740, North Adelaide, South Australia 5006, Australia; and ⁵Department of Earth, Ocean and Atmospheric Sciences, 2020–2207 Main Mall, University of British Columbia, Vancouver, British Columbia, Canada

Abstract

Orthoamphibole, clinoamphibole and magnetite are common minerals in altered rocks associated spatially with Palaeoproterozoic volcanogenic massive sulfide (VMS) deposits in Colorado, USA and metamorphosed to the amphibolite facies. These altered rocks are dominated by the assemblage orthoamphibole (anthophyllite/gedrite)–cordierite–magnetite±gahnite±sulfides. Magnetite also occurs in granitoids, banded iron formations, quartz garnetite, and in metallic mineralisation consisting of semi-massive pyrite, pyrrhotite, chalcopyrite, and sphalerite with subordinate galena, gahnite and magnetite; amphibole also occurs in amphibolite. The precursor to the anthophyllite/gedrite–cordierite assemblages was probably the assemblage quartz–chlorite formed from hydrothermal ore-bearing fluids (~250° to 400°C) associated with the formation of metallic minerals in the massive sulfide deposits.

Element–element variation diagrams for amphibole, magnetite and ilmenite based on LA-ICP-MS data and Principal Component Analysis (PCA) for orthoamphiboles and magnetite show a broad range of compositions which are primarily dependent upon the nature of the host rock associated spatially with the deposits. Although discrimination plots of Al/(Zn+Ca) vs Cu/(Si+Ca) and Sn/Ga vs Al/Co for magnetite do not indicate a VMS origin, the concentration of Al+Mn together with Ti+V and Sn vs Ti support a hydrothermal rather than a magmatic origin for magnetite. Principal Component Analyses also show that magnetite and orthoamphibole in metamorphosed altered rocks and sulfide zones have distinctive eigenvalues that allow them to be used as prospective pathfinders for VMS deposits in Colorado. This, in conjunction with the contents of Zn and Al in magnetite, Zn and Pb in amphibole, ilmenite and magnetite, the Cu content of orthoamphibole and ilmenite, and possibly the Ga and Sn concentrations of magnetite constitute effective exploration vectors.

Keywords: magnetite; amphiboles; metamorphism; exploration guides; volcanogenic massive sulfide deposits; Colorado; USA

(Received 11 May 2023; accepted 28 August 2023; Accepted Manuscript published online: 11 September 2023; Associate Editor: David Good)

Introduction

Trace-element studies of individual minerals (e.g. magnetite, McCurdy *et al.*, 2022; chromite, Pagé and Barnes, 2009; gahnite, O'Brien *et al.*, 2015) have been used increasingly to explore for various ore deposit types, to aid in classification of a given ore type, and to determine the provenance of the mineral of interest. What is less common in the literature is the application of trace-element compositions of multiple minerals from a given ore deposit/district to evaluate these same parameters. Some

exceptions include using trace-element studies of chlorite, epidote and pyrite in vectoring towards the Resolution porphyry Cu–Mo deposit, Arizona (Cooke *et al.*, 2020), and investigations in ferromagnesian silicates and oxides in the Cambrian Kanmantoo metallogenic district, South Australia, where chlorite, biotite, garnet, gahnite, magnetite and ilmenite were analysed in ore and altered rocks in metamorphosed sedimentary exhalative/inhalative Cu–Au (Pollock *et al.*, 2018) and Pb–Zn–Ag–(Cu–Au) (Tott *et al.*, 2019) deposits. These studies highlight the utility of trace-element compositions of multiple minerals as vectoring tools in exploring for ore deposits.

Some minerals, such as magnetite, have trace-element compositions that are dependent on temperature, source rock/fluid composition, oxygen and sulfur fugacity, silicate and sulfide activity, host-rock buffering, re-equilibration processes and intrinsic crystallographic controls (Nadoll *et al.*, 2014). These compositions are

Corresponding author: Paul G. Spry; Email: pgspry@iastate.edu

Cite this article: Spry P.G., Berke E.H., Layton-Matthews D., Voinot A., Heimann A., Teale G.S. and von der Handt A. (2024) The trace-element compositions of amphibole, magnetite and ilmenite as potential exploration guides to metamorphosed Proterozoic Cu–Zn±Pb±Au±Ag volcanogenic massive sulfide deposits in Colorado, USA. *Mineralogical Magazine* 88, 61–89. <https://doi.org/10.1180/mgm.2023.69>

© The Author(s), 2023. Published by Cambridge University Press on behalf of The Mineralogical Society of the United Kingdom and Ireland. This is an Open Access article, distributed under the terms of the Creative Commons Attribution licence (<http://creativecommons.org/licenses/by/4.0/>), which permits unrestricted re-use, distribution and reproduction, provided the original article is properly cited.

generally related to ore-forming processes that are distinct for different ore deposit types. Hence the trace-element compositions of magnetite can be used to characterise a particular ore type (e.g. magnetite-bearing ore deposits including Ni–Cu–PGE, banded iron formation (BIF), iron oxide–Cu–Au (IOCG), skarn, porphyry Cu, Fe–REE–Nb, Cu–Au–Fe, iron oxide–apatite, and volcanogenic massive sulfide deposits (VMS)) as has been shown by Dupuis and Beaudoin (2011) and Bédard *et al.* (2022). Of these deposit types, there is a general paucity of trace-element information for minerals from metamorphosed VMS deposits, with magnetite being the exception for which several studies have been undertaken (Singoyi *et al.*, 2006; Kamvong *et al.*, 2007; Dupuis and Beaudoin, 2011; Makvandi *et al.*, 2013; 2016a, 2016b; Maghfouri *et al.*, 2021; Bédard *et al.*, 2022; Sun *et al.*, 2022). Makvandi *et al.* (2016a) in evaluating 15 VMS deposits showed that the composition of magnetite was related to the composition of the host bedrocks, parental magma, coexisting minerals, temperature of the ore fluid and oxygen fugacity. They also showed that the Al, Co, Mg, Ni, Si, Ti, Zr and Zn concentrations of magnetite are generally lower than in other ore deposit types.

In central Colorado, USA, the area of this investigation, the composition of metamorphosed altered rocks in small VMS deposits varies, but is principally dominated by the assemblage orthoamphibole (anthophyllite/gedrite)–cordierite–magnetite \pm gahnite \pm sulfides (Berke *et al.*, 2023). Cordierite–anthophyllite/gedrite assemblages in metamorphosed alteration pipes have long been identified in and adjacent to metamorphosed massive sulfide deposits and are used as exploration guides for finding VMS deposits (e.g. Blue Hill, USA – Lindgren, 1925; Falun, Sweden – Wolter and Seifert, 1984, Kampmann *et al.*, 2018; Outokumpu, Finland – Treloar *et al.*, 1981; Gullbridge, Canada – Upadhyay and Smitheringale, 1972). Although the major-element composition of cordierite–orthoamphibole rocks have been reported previously in the literature (Orijärvi, Smith *et al.*, 1992), including the metamorphosed massive sulfide deposits in central Colorado (Berke *et al.*, 2023), the trace-element compositions of amphibole, magnetite and ilmenite in such rocks have not been determined previously.

Contrasting models have been proposed to explain the origin of the massive sulfide deposits in Colorado including: VMS (Drobeck, 1981; Sheridan and Raymond, 1984), carbonate-replacement skarn (Salotti, 1965), and high-temperature fractionation of base and precious metals from peraluminous granitoids (Kleinhans and Swan, 2022). However, recent geological, mineralogical and geochemical data favour the VMS model (Berke *et al.*, 2023).

This investigation of clin amphibole, orthoamphibole, magnetite and ilmenite in central Colorado will be used to assess: (1) whether or not the trace-element compositions of these minerals vary sufficiently and consistently such that they can be used as pathfinders to ore; and (2) to evaluate compositional discrimination diagrams that have been published previously to help in understanding the conditions of formation of magnetite.

Regional geology

Metamorphosed massive Cu–Zn–Au–(Pb–Ag) deposits occur in the central part of Colorado in the 300 km wide so-called transitional zone between the Yavapai and Mazatzal tectonic provinces (Figs 1, 2). The Yavapai Province (2.0–1.8 Ga) is an aggregate of juvenile arc terranes, whereas the Mazatzal Province (~1.8–1.7 Ga,

Bennet and DePaolo, 1987) is a microcontinent accreted onto the southern margin of the Yavapai Province at ~1.65–1.60 Ga (e.g. Duebendorfer *et al.*, 2015). This accretion was associated with extension, the development of ductile shear zones, and at least three folding events. Isoclinal folds are associated with the first deformation event, whereas the second and third events generated large open folds, which trend generally northwest to north. Calc-alkaline to peraluminous granitoids occur throughout central Colorado and were emplaced from 1.9 to 1.1 Ga (e.g. Bickford *et al.*, 1989; Siddoway *et al.*, 2000). The calc-alkaline granitoids intruded basement rocks at 1.9 to 1.7 Ga whereas the peraluminous plutons were intruded at ~1.7 Ga (Anderson and Cullers, 1999; Premo and Fanning, 2000). A-type granitic batholiths occurred at ~1.45 to 1.35 Ga followed by a later event (1.1 Ga) associated with the formation of the Pikes Peak batholith (Hedge, 1970). The base metal deposits occur in a package of metasedimentary, granitoids and bimodal metavolcanic rocks (Fig. 2). Pb–Pb radiometric age determinations for galena of between 1.8 and 1.7 Ga from massive sulfides were reported by Sheridan and Raymond (1984). Metamorphosed massive sulfide deposits are associated spatially with the peraluminous granitoids (Kleinhans and Swan, 2022), though these granitoids probably have no genetic relationship to the sulfide-forming events on the basis of structural relationships of the host rocks to the sulfide deposits (Berke *et al.*, 2023).

Although the mineralogy and textures observed in Proterozoic rocks in Colorado mostly reflect regional metamorphism associated with the Yavapai orogeny (1.71 to 1.68 Ga; Karlstrom *et al.*, 2001), reheating and superimposed metamorphism to the amphibolite facies is also associated with the younger Mazatzal orogeny (1.65 to 1.60 Ga; Magnani *et al.*, 2004). Rocks in central-southern Colorado were mostly metamorphosed to the middle to upper amphibolite facies with upper greenschist- to lower amphibolite-facies metamorphism being reached in Paleoproterozoic rocks associated with the Gunnison VMS district west of the studied deposits (Drobeck *et al.*, 1981; Sheridan *et al.*, 1981). Of note is that chlorite–sericite–quartz alteration occurs in some of the deposits in this district (e.g. Vulcan–Good Hope, Drobeck *et al.*, 1981), which is the probable precursor assemblage to the orthoamphibole–cordierite alteration that is associated spatially and genetically with the deposits investigated in this work that were subsequently metamorphosed to the upper amphibolite facies.

Local geology

Samples were obtained from ten massive sulfide deposits (Betty, Cinderella, Cotopaxi, Dawson, El Plomo, Evergreen, Green Mountain, Horseshoe, Swede and Wolverine) with the emphasis being on those deposits along the Dawson–Green Mountain Trend, near Cañon City (Fig. 2). Details of the geological setting and mineralogy of the cordierite–gedrite rocks at Evergreen are given in Heimann *et al.* (2006), whereas general information on the geological setting of VMS deposits in Colorado are given in Heinrich (1981), Sheridan and Raymond (1984), Spry *et al.* (2022) and Berke *et al.* (2023). The geological characteristics of these massive sulfide deposits are summarised in Table 1.

All of the metamorphosed massive sulfide deposits in Colorado are considered as small, with the largest being the Sedalia deposit, which contained ~1.2 million tonnes of ore at 3.25% Cu, 5.6% Zn, 23 g/t Ag and 0.3 g/t Au (Heinrich, 1981). They were mined mostly between 1880 and 1900, with the Betty deposit being mined in the 1950s. Metallic minerals in

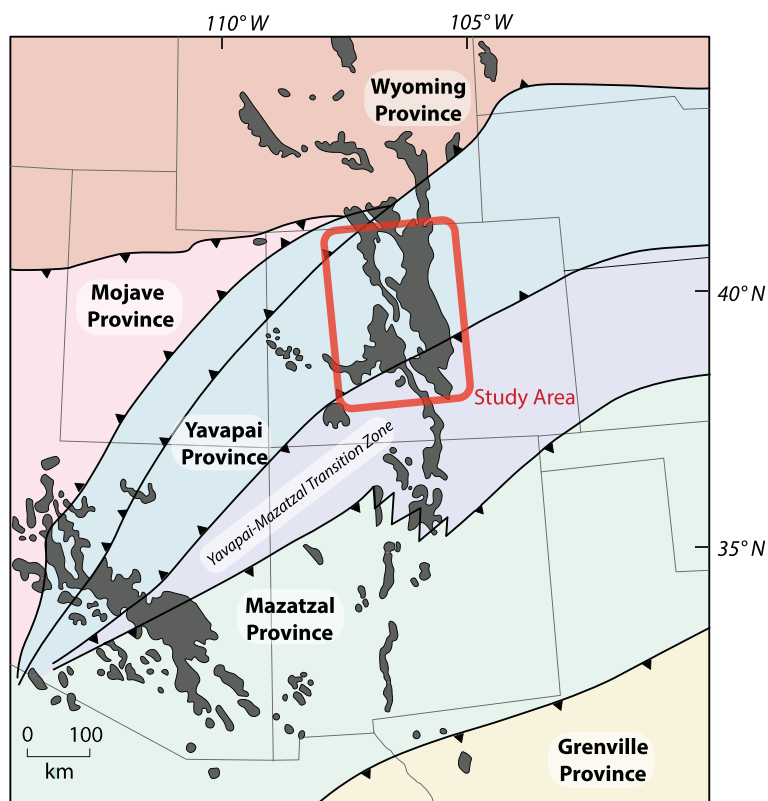


Figure 1. Regional geological map of the southwestern United States. Major crustal provinces, transition zones, inferred boundaries and deformation fronts are delineated (modified after Jones *et al.*, 2010). An inset map showing the study area (see Fig. 2) is also indicated.

these deposits are dominated by chalcopyrite, sphalerite, pyrite, pyrrhotite and galena, with subordinate amounts of zincian spinel, magnetite, ilmenite, hematite, rutile and, in some locations (e.g. Cotopaxi), minor molybdenite and scheelite. Host rocks to the sulfide deposits consist mainly of biotite–muscovite schists, sillimanite–biotite gneiss, amphibolite and nodular sillimanite rocks, with calc–silicate rocks being present locally. The deposits studied here were metamorphosed to the sillimanite zone of the upper amphibolite facies. At least three folding events have affected most deposits, reflecting regional fold events, together with deformation zones (prominent along the Dawson–Green Mountain Trend), and late-stage faults (Spry *et al.*, 2022; Berke *et al.*, 2023).

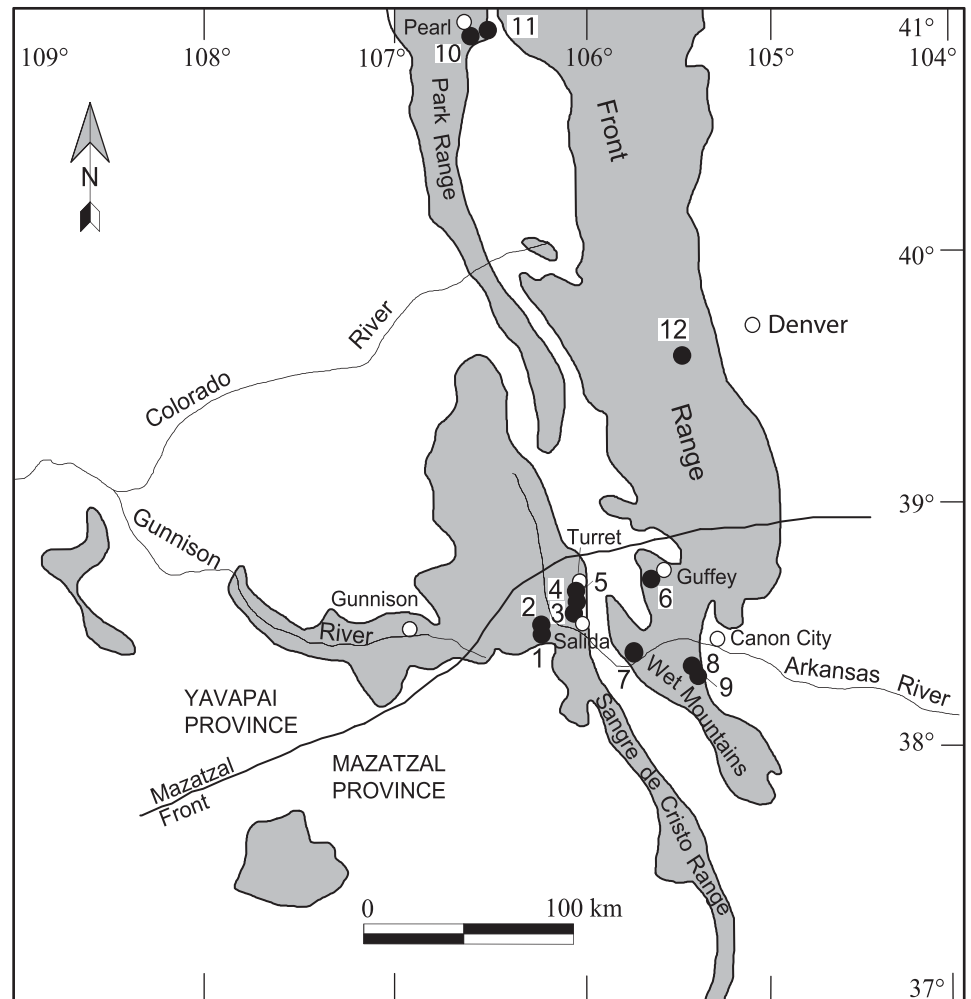
Metamorphosed altered rocks

The most common mineralised rock types in the deposits consist of various combinations of the following: garnet–biotite–muscovite schist, garnet gneiss, chlorite schist, nodular sillimanite rock, calc–silicate rock, iron formation, quartz garnetite, and rocks consisting almost entirely of gahnite, orthoamphibole/clinoamphibole, or chlorite. Narrow zones, commonly less than a few metres in width, of metamorphosed altered rocks occur in both the footwall and hanging wall of most deposits. However, footwall alteration pipes, which are commonly associated with VMS deposits, are absent. This is probably due to the isoclinal folding affecting rocks associated with some of the deposits and the presence of a low-angle deformation zone that parallels bedding. Stratabound metamorphosed altered rocks are mineralogically varied but commonly consist of nodular sillimanite rocks (Spry *et al.*, 2022), orthoamphibole–cordierite±gahnite-bearing rocks (Fig. 3a–c), locally abundant rhodonite–actinolite–quartz

rock at Cinderella, anthophyllite–cordierite–cummingtonite–gahnite–garnet±pigeonite±hornblende at Green Mountain, and anthophyllite–chlorite–biotite–talc/serpentine–quartz and biotite–garnet–anthophyllite–cordierite±gahnite±hornblende±tremolite±magnetite rocks at Dawson. A horizon of gedrite–cordierite gneiss, up to 40 m in width which extends intermittently for ~300 m, occurs in a sequence of sillimanite–biotite gneisses near Evergreen, which Heimann *et al.* (2006) considered to be a stratabound zone of metamorphosed hydrothermal alteration.

Amphibole, magnetite and ilmenite are present in ore, as well as various types of metamorphosed altered rocks, particularly cordierite–orthoamphibole±gahnite-bearing rocks (Fig. 3a–c). Orthoamphibole are commonly bladed and vary in grain size up to 6 cm in length. They can be intergrown with clinoamphibole (hornblende, cummingtonite, grunerite and tremolite), gahnite, phlogopite, cordierite, quartz and base-metal sulfides (Berke *et al.*, 2023). Magnetite is a common accessory in ore zones intergrown with sulfides, and in metamorphosed altered rocks (Fig. 3a–d), amphibolite (Fig. 3e), quartz–magnetite (i.e. iron formation), and quartz–garnet–magnetite rocks (Fig. 3f). Although magnetite might contain small inclusions of quartz, it can also contain lamellae of ilmenite (Fig. 3g), and in rare instances, hercynite. Ilmenite is considerably less common than magnetite, but is present as a minor accessory in amphibolite, and gahnite-bearing and gahnite-absent metamorphosed altered rocks along the Dawson–Green Mountain Trend. Ilmenite in gedrite–cordierite rocks at Evergreen occurs as xenomorphic to subhedral grains up to 0.5 mm in length in a corona of aluminous minerals (hercynite, corundum and högbomite), as well as inclusions in cordierite, staurolite and hercynite (Heimann *et al.*, 2006). Where present, ilmenite in these rocks locally contains tiny exsolutions of titaniferous hematite up to 5 µm in length (Fig. 3h).

Figure 2. General map of southern Colorado, USA, showing the extent of Proterozoic rocks (grey shaded pattern; after Sheridan and Raymond, 1984; Heimann *et al.*, 2005), terrane boundaries (after Shaw and Karlstrom, 1999), and location of metamorphosed massive sulfide deposits: 1 Bon Ton, 2 Cinderella, 3 Sedalia, 4 Ace High/Jackpot, 5 Independence, 6 Betty (Lone Chimney), 7 Cotopaxi, 8 Green Mountain, 9 Dawson-Grape Creek trend (which includes El Plomo and Horseshoe), 10 Wolverine, 11 Swede and 12 Evergreen hydrothermal alteration zone. The location of the Mazatzal Deformation Front is derived from Shaw and Karlstrom (1999).



Amphibolite from Green Mountain consists primarily of coarse hornblende, plagioclase, quartz and garnet with minor biotite, magnetite and ilmenite with trace pyrite and chalcopyrite. Ilmenite occurs as anhedral to subhedral isolated grains up to 0.6 mm in length primarily in contact with hornblende and plagioclase but nowhere in contact with magnetite. Ilmenite in biotite–gahnite rock from Green Mountain is also isolated from magnetite and occurs as anhedral grains (up to 0.7 mm) in biotite and gahnite. At El Plomo, ilmenite (up to ~0.5 mm in length) formed as subhedral grains in an anthophyllite–plagioclase–sulfide rock in contact with anthophyllite, plagioclase and pyrite.

Analytical methods

Over 200 polished thin-sections were examined with a dual reflected and transmitted light Olympus BX–60 microscope and a scanning electron microscope (SEM). Major-element compositions of amphibole were obtained using a JEOL JXA–8530F Plus Field Emission Electron Probe Microanalyser at the University of Minnesota. Analyses of silicates were conducted using a 15 kV accelerating voltage with a 20 nA beam current, and a 1–2 μm spot size. Mineral standards included hornblende (Si, Al, Mg, Ca), ilmenite (Ti, Fe), albite (Al, Na), spessartine (Al, Mn), pyrope (Si, Mg), K-feldspar (K), gahnite (Zn, Al), tugtupite (Cl) and apatite (F). The mineralogy of amphibole, magnetite and ilmenite-bearing samples are listed in Table 2.

A FEI Quanta-250 SEM in the Materials Analysis and Research Laboratory at Iowa State University was used to evaluate the possibility of exsolution, lamellae and intergrowths among minerals in the system Fe–Al–Ti–O (i.e. magnetite, ilmenite, hematite and hercynite). This is equipped with standard secondary and back-scattered electron detectors, together with an Oxford Aztec energy-dispersive X-ray analysis system. Analyses were done using a 15 kV accelerating voltage.

Trace-element compositions of orthoamphibole ($n=139$), clinoamphibole ($n=40$), magnetite ($n=160$) and ilmenite ($n=82$) in selected polished thin-sections were obtained with a ThermoScientific X Series 2^o quadrupole ICP–MS coupled to a New Wave/ESI 193-nm ArF Excimer laser ablation-inductively coupled plasma (LA–ICP)–mass spectrometer at the Queen’s Facility for Isotope Research at Queen’s University, Kingston, Ontario, Canada. These minerals were ablated at a beam diameter of 50 μm with a laser repetition of 10 Hz. The standards used were GSC-1G, GSD-1G, GSE-1G, NIST612 and NIST610, which were ablated before and after each set of samples, and preferred values sourced from GeoReM (Guillong *et al.*, 2005; Jochum *et al.*, 2005, 2011). A calibration curve using NIST610 and NIST612 (Pearce *et al.*, 1997) was used to correct for variations in laser yield. Before each analysis, 20 s of gas blank was measured to establish background values. Data were reduced using the Thermo Electron Corporation’s *PlasmaLab* software. Sites chosen to ablate attempted to try and avoid visible mineral inclusions. However,

Table 1. Summary of geological characteristics of the metamorphosed massive sulfide deposits investigated, Colorado, USA.

Deposit	Grades, reserves, past production, metallic minerals	Metamorphic grade, structure	Country rocks	Mineralised rocks	References
Betty (Lone Chimney)	Past production: 3,900 kg Cu, 1680 kg Pb, 1,680 kg Zn, 4.76 kg Ag, 312g Au, Py, Ccp, Sp, Gn, Pyh, Py, Bn, Cv, Ilm, Mag, Hem	Upper amphibolite, shear and fault have disrupted the orebody	Bt gneiss, Qz-Ms schist, Qz-Crd-Sil gneiss, Amphibolite	Qz-Crd-Sil gneiss, Nodular Sil gneiss, Calc-silicate gneiss, Crd-Ath rock, Ghn rock, Act-Bt rock, Ath rock, Qz-Crd rock	Heinrich (1981), Heimann <i>et al.</i> (2005)
Cinderella	Unknown grade, best sample from dump: 1.9 % Cu, 6.4 % Zn 47 g/t Ag; Sp, Ccp, Gn, Py	Upper amphibolite, complex folds, three deformation events	Sil-Qz-Ms gneiss, Qz-Bt-Ep gneiss, Amphibolite, Grt gneiss	Nodular Sil gneiss, Bt-Grt schist, Bt gneiss, Ms schist, Ath-Crd rock, Quartzite	Heinrich (1981), Heimann <i>et al.</i> (2005)
Cotopaxi	Past production: 0.01 of 1337 tonnes Zn, 83 tonnes Cu, 71 tonnes Pb, 301 kg Ag, 4.5 kg Au; Sp, Ccp, Gn, Pyh, Py, Mrc, Rt, Ilm, Mol, Cv, Mag	Upper amphibolite, orebody hosted in monocline	Qz-Bt-Fsp-Sil gneiss, Nodular Sil schist, Hbl gneiss, Bt schist, Calc-silicate gneiss, Granite gneiss, Pegmatite	Ghn-Ath-Crd rock, Nodular Sil-Bt rock, Ath-Bt gneiss, Ghn-Qz-Grt rock, Pegmatitic Ghn-Bt rock, Chl schist, Qz-Bt garnetite	Lindgren (1908), Salotti (1965), Heimann <i>et al.</i> (2005)
Dawson	No production, ~4250 kg Au @ 5g/t; Py, Pyh, Ccp, Sp, Mag, Ghn	Upper amphibolite	Granite gneiss, Bt schist, Qz-Bt-Grt gneiss, Amphibolite, Metagabbro, Pegmatite	Qz-Bt±Grt gneiss, Fsp-Bt-Mag-Qz gneiss, Qz-Bt-Sil gneiss	Berke <i>et al.</i> (2023), Kleinhans and Swan (2022)
El Plomo	Best drill hole intersections: 9.2% Pb and 0.7 % Cu over 1.6 m and 4.6 % Zn, 0.2 % Cu, and 0.2 % Pb over 1.4 m; Py, Pyh, Sp, Gn, Ccp, Mag, Ghn	Upper amphibolite	Qz-Fsp-Bt±Crd±Sil±Grt rock, Amphibolite, Granite gneiss, Bt-Qz monzodiorite	Qz-Ath-Crd-Bt rock, Qz-Bt-Chl-Ksp gneiss	Aiken (1981)
Evergreen	No production, Ccp, Sp, Pyh	Upper amphibolite	Sil-Ms-Qz-Alm gneiss, Ged-Alm-Crd gneiss, Amphibolite, Calc-silicate rock	Ged-Alm-Crd gneiss, Nodular Sil rock	Heimann <i>et al.</i> (2006)
Green Mountain	Best drill hole intersection: 18.1 % Cu and 4.3 % Zn over 1.5 m, Ccp, Py, Sp, Gn, Mol, Pyh, Ilm, Hem, Rt	Upper amphibolite, broad NE-SW trending folds	Qz-Fsp gneiss, Qz-Crd-Grt-Bt gneiss, Migmatite, Ath-Crd rock, Nodular Sil rock, Sil gneiss, Hbl-Bt-Crd gneiss, Amphibolite	Nodular Sil rock, Qz-Grt gneiss, Ath-Crd-Ghn rock, Grt Amphibolite, Grt-Sil gneiss, Qz-garnetite, Qz-Bt gneiss, Grt-bearing pegmatite	Ririe (1981), Heimann <i>et al.</i> (2005)
Horseshoe	Best drill hole intersection: 4.4 % Zn over 3 m; Sp, Gn, Ccp, Mag, Ghn, Po	Upper amphibolite-granulite	Qz-Fsp-Bt gneiss, Migmatite, Amphibolite, Granite gneiss, Bt-Qz monzodiorite	Qz-Bt gneiss, Ath-Crd-Ghn rock	This study
Swede	No production, Ccp, Cc, Bn	Upper amphibolite	Qz-Grt-Bt gneiss, Amphibolite, Chert, Banded iron formation	Cum-Qz-Hbl-Grt-Mag rock, Nodular Sil rock	This study, Sheridan and Raymond (1984)
Wolverine	No production, Ccp, Cc, Bn	Upper amphibolite	Qz-Grt-Bt gneiss, Amphibolite, Mafic fragmental rocks	Qz-Pl-Bt-Grt-Crd-Mag-sulfide rock, Nodular Sil rock	This study, Sheridan and Raymond (1984)

Notes: Abbreviations after Warr (2021).

if inclusions were ablated these were removed from the obtained data, which were then integrated to give an average value and error for each element analysed, in parts per million. For magnetite and ilmenite, iron (^{57}Fe) was used as an internal standard and ^{55}Mn was used as the internal standard for amphiboles, both of which were obtained from electron microprobe analyses. For orthoamphiboles and clinoamphiboles, 59 elements were analysed: ^{27}Al , ^{11}B , ^{209}Bi , ^{44}Ca , ^{111}Cd , ^{59}Co , ^{52}Cr , ^{63}Cu , ^{163}Dy , ^{166}Er , ^{57}Fe , ^{71}Ga , ^{157}Gd , ^{72}Ge , ^{165}Ho , ^{39}K , ^{139}La , ^{175}Lu , ^7Li , ^{23}Na , ^{93}Nb , ^{31}P , ^{208}Pb , ^{141}Pr , ^{45}Sc , ^{29}Si , ^{118}Sn , ^{88}Sr , ^{159}Tb , ^{47}Ti , ^{169}Tm , ^{51}V , ^{89}Y , ^{172}Yb and ^{66}Zn , which were generally above detection limits, whereas ^{107}Ag , ^{75}As , ^{137}Ba , ^9Be , ^{140}Ce , ^{133}Cs , ^{153}Eu , ^{178}Hf , ^{115}In , ^{95}Mo , ^{146}Nd , ^{60}Ni , ^{195}Pt , ^{85}Rb , ^{185}Re , ^{121}Sb , ^{77}Se , ^{147}Sm , ^{181}Ta , ^{232}Th , ^{205}Tl , ^{238}U , ^{182}W and ^{90}Zr were mostly near or below detection limits. Detection limits for the oxides

(magnetite and ilmenite) and amphiboles were determined using the data software package *Iolite* (Paton *et al.* 2011; Wagner *et al.*, 2023) and given in Supplementary Table S1. A notable difference between the trace-element concentrations of orthoamphiboles and clinoamphiboles is that the light rare earth elements (LREE) are generally below detection limits for orthoamphiboles whereas all REE are mostly above detection limits for clinoamphiboles. The following trace elements for magnetite and ilmenite were above detection limits: ^{27}Al , ^{44}Ca , ^{59}Co , ^{52}Cr , ^{63}Cu , ^{71}Ga , ^{72}Ge , ^{24}Mg , ^{55}Mn , ^{60}Ni , ^{45}Sc , ^{29}Si , ^{118}Sn , ^{47}Ti , ^{51}V , ^{66}Zn and ^{90}Zr , whereas ^{209}Bi , ^{178}Hf , ^{115}In , ^{95}Mo , ^{93}Nb , ^{208}Pb , ^{185}Re and ^{181}Ta were generally below the limits of detection. The elements Si, Ca and the REE in magnetite and ilmenite were included primarily for screening purposes to identify mineral inclusions, which might be submicroscopic in size or below

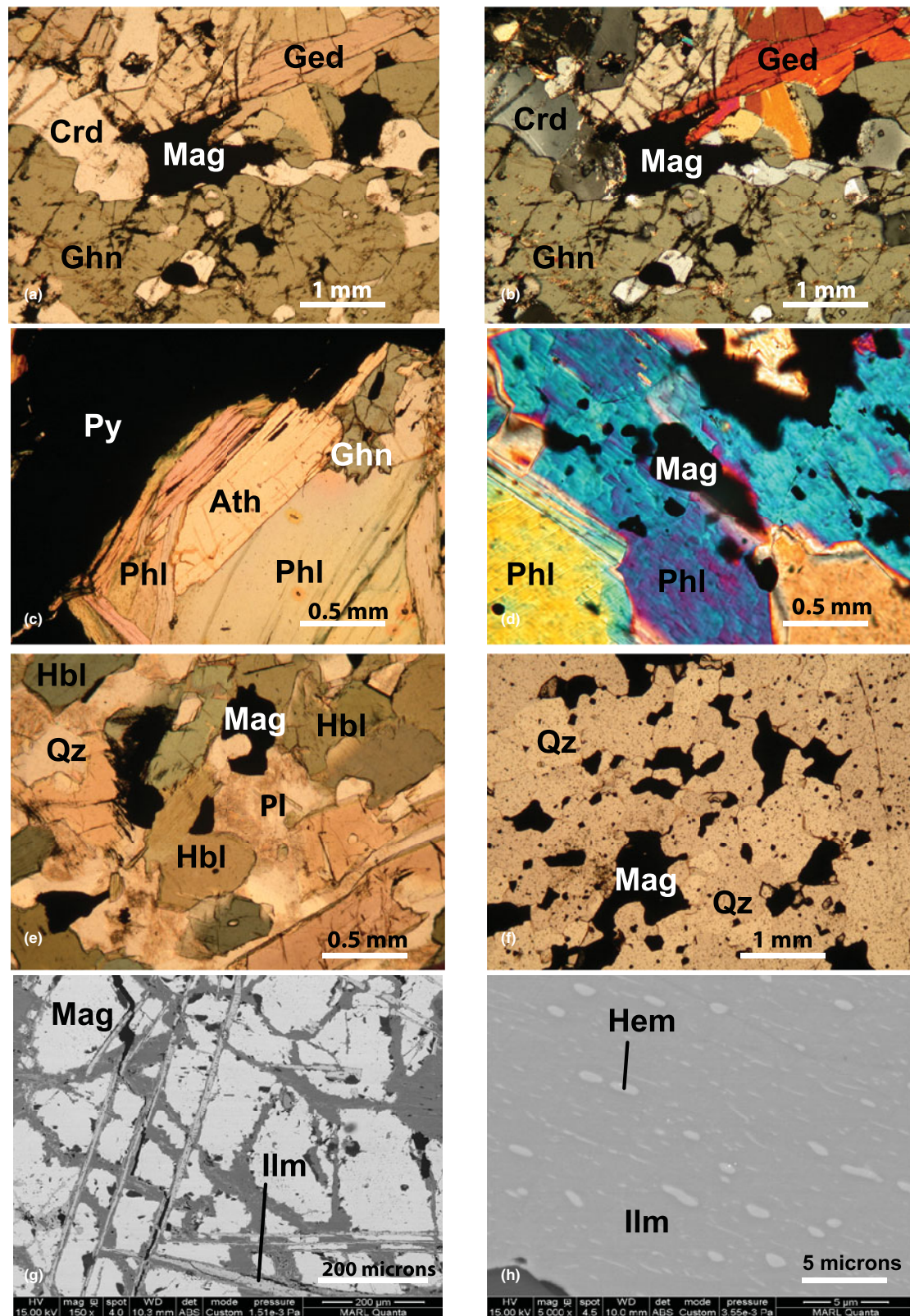


Figure 3. Polished thin-section photomicrographs of metamorphosed altered rocks and amphibolite associated with massive sulfide deposits in Colorado. (a) Anthophyllite (Ath) intergrown with cordierite (Crd), magnetite (Mag) and gahnite (Ghn) (Dawson, TVD-40B), transmitted light. (b) Same view as image (a) in cross-polarised light. (c) Anthophyllite, phlogopite (Phl) and gahnite intergrown with pyrite (Py) (Wolverine, 99CO-119), transmitted light. (d) Magnetite inclusions in phlogopite (El Plomo, TVD-126), cross-polarised light. (e) Hornblende (Hbl), plagioclase (Pl), magnetite and quartz in amphibolite (Green Mountain, AHCO-28), transmitted light. (f) Quartz-magnetite assemblage in banded quartz-banded-garnet rock; interpreted as an exhalative unit (Green Mountain, GM-20-27), transmitted light. (g) Back-scattered electron image of magnetite showing cross-cutting ilmenite lattice in biotite-gahnite altered rock (Green Mountain, TVD18-89). (h) Back-scattered electron image of ilmenite with fine exsolutions of titaniferous hematite in gedrite-cordierite-garnet gneiss (Evergreen, 99CO-65B). Mineral abbreviations after Warr (2021).

Table 2. Mineralogy of amphibole, magnetite and ilmenite-bearing samples analysed by LA-ICP-MS.

Deposit	Sample No.	Mineral	Location	Lithology	Assemblage*
Dawson	TVD-18	Ath, Ged	WG-16-27 823	Ged-Ghn-Chl alt. rock	Ged, Chl, Ghn, Crd, Tlc ² , Py, Ccp, Sp
Dawson	TVD-24	Ath	Outcrop	Ath alt. rock	Ath, Ms
Dawson	TVD-26	Mag	Outcrop	Crd-Bt alt. rock	Qz, Pl, Crd, Bt, Sil, Ap, Mag, Ilm ¹ , Py ¹
Dawson	TVD-30	Ath	Outcrop	Ath alt. rock	Ath, Phl
Dawson	TVD-53	Ged	WG-13-14 57.5	Ath-Ghn rock	Ath, Ghn, Bt, Sp
Dawson	TVD-74	Ath	DA-18-16 612	Sulfide zone	Phl, Po, Pyh, Ghn, Ms, Crd, Sp, Pl, Ccp, Chl, Mnz
Dawson	TVD-93	Mag	GC-44 762.2	Qz-Bt-Crd alt. rock	Qz, Bt, Crd, Pl, Ap, Ser ² , Mag, Ilm ¹
Dawson	TVD-129	Mag	DA-18-16 652	Qz-Pl-Crd alt. rock	Qz, Pl, Crd, Or, Mag, Py, Pyh, Sp ¹ , Grt ¹ , Ccp ¹
Dawson	TVD-130	Mag	DA-18-16 653	Sulfide zone	Qz, Crd, Or, Bt, Mag, Py, Pyh, Ccp, Gth ² , Ilm ¹
Dawson	TVD-131	Mag	DA-18-16 654	Qz-Grt-Crd rock	Qz, Grt, Crd, Pl, Bt, Mag
Dawson	TVD-40B	Mag	GC-8 153	Bt-Qz-Ath-Ghn alt. rock	Bt, Qz, Ath, Ghn, Grt, Mag, Hbl, Py, Ccp, Tur ¹ , Hgb ¹
El Plomo	TVD19-25	Hbl	GC-9 204	Sulfide zone	Bt, Crd, Sp, Py, Qz, Ms, Hbl, Ccp, Ser ²
El Plomo	TVD19-43	Ged, Hbl	GC-8 187	Sulfide zone	Hbl, Ath, Qz, Pl, Crd, Ccp, Py, Gn, Pyh, Ilm
El Plomo	TVD-126	Mag	GC-9 184.3	Sulfide zone	Qz, Bt, Ms, Grt, Hbl, Py, Sp, Ccp, Pyh, Mag, Mnz
El Plomo	TVD19-31	Mag	GC-9 251	Pl-Hbl alt. rock	Pl, Hbl, Qz, Ap, Ser ² , Gn, Mag, Py, Ccp, Ilm ¹
El Plomo	TVD19-41	Mag, Ilm	GC-8 172	Ath-Pl alt. rock	Ath, Pl, Qz, ilm, Py, Ccp, Gn, Bt, Ser ² , Mag ¹
El Plomo	TVD19-59	Ath	Float	Sulfide zone	Ath, Pl, Qz, Crd, Gn, Ccp, Mag, Ilm, Tlc ² , Py ² , Ser ² , Cal ²
Horseshoe	TVD19-48	Mag, Ilm	GC-2 52	PBU	Qz, Mc, Ms, Ser ² , Bt, Crd?, Mag, Hc ¹
Green Mt.	EHB-20-15	Mag	Outcrop	Amphibolite	Hbl, Qz, Or, Ep, Mag, Py ¹
Green Mt.	TVD19-89	Mag, Ilm	Float	Bt-Ghn alt. rock	Bt, Ghn, Mag, Ap, Ilm, Mnz, Chl ^{1,2} , Py ¹ , Ccp ¹
Green Mt.	TVD19-96	Hbl	Outcrop	Hbl-Ghn alt. rock	Hbl, Ghn, Crd, Sp, Ccp, Phl
Green Mt.	GM-20-27	Mag	Float	Grt-Qz rock	Qz, Grt, Mag
Green Mt.	AHCO-25	Ilm	Float	Ath-Ghn alt. rock	Ath, Ghn, Crd, Ccp, Ilm
Green Mt.	AHCO-29	Mag, Ilm	Outcrop	Amphibolite	Ath, Grt, Hbl, Qz, Pl, Mag, Ilm, Bt ¹ , Py ¹ , Ccp ¹
Green Mt.	AHCO-35	Ilm	Float	Ghn alt. rock	Ghn, Crd, Tlc ² , Ms ² , Ilm
Cinderella	99CO-3	Ath	Outcrop	Ghn alt. rock	Ghn, Chl, Ath, Phl, Sil
Cotopaxi	99CO-12	Ath	Outcrop	Ath-Ghn alt. rock	Ath, Ghn, Phl, Zrn, Rt
Cotopaxi	EHB-20-36	Mag	Outcrop	Altered greywacke	Qz, Mc, Bt, Grt, Ms, Mag, Py ¹
Betty	99CO-89	Ath	Outcrop	Ath-Ghn alt. rock	Ath, Ghn, Chl, Rt, Ilm
Betty	99CO-91	Mag	Outcrop	Cum alt. rock	Cum, Ol, Rt, Mag, Cpx, Ghn
Evergreen	99CO-63	Ilm	Outcrop	Ged-Crd rock	Ged, Crd, Grt, Qz, Ilm, Bt, Chl ² , Ser ² , Sp ¹ , Py ¹ , Ccp ¹
Evergreen	99CO-65B	Ilm	Outcrop	Ged-Crd rock	Ged, Crd, Grt, Ilm, Bt, Chl ² , Ser ² , Hc ¹ , Crn ¹ , Hgb ¹
Swede	99CO-110	Mag	Outcrop	Cum-Hbl-Grt ¹ alt. rock	Cum, Qz, Hbl, Grt, Mag, Hem ^{1,2}
Wolverine	99CO-119	Mag	Outcrop	Qz-Pl-Bt-Ath-Grt alt. rock	Qz, Pl, Bt, Ath, Grt, Crd, Or, Mag, Py, Sp, Pyh, Ccp, Grt

Notes: Mineral abbreviations after Warr (2021); alt = altered.

¹Trace amount; ² secondary mineral; * listed in approximate order of abundance

the surface of the polished thin-section (Dare *et al.*, 2014; Nadoll *et al.*, 2014).

Principal Component Analysis

Principal Component Analysis (PCA), which is a statistical method that extracts the dominant sources of variation in a multi-variate dataset (Davis, 2002; Jolliffe and Cadima, 2016), was used here to discriminate the trace-element compositions of magnetite and orthoamphibole. A PCA allows trends in large data sets to be distinguished. In plotting a PCA, the relative direction and length of each vector represents the relationship of that element to the others: longer vectors represent a stronger contribution to the principal component. Elements with arrows pointing in the same direction are related positively to each other, elements with arrows pointing in opposite directions are related negatively to each other, and elements with arrows at right angles to each other are not related. A PCA for ilmenite and clinoamphiboles was not done due to the limited number of compositional data obtained.

For the present study, we included censored geochemical data, which contains values below detection limits for some elements. The trace-element data for magnetite and orthoamphibole were pre-treated using the method of Croghan and Egeghy (2003) such that up to 40% censored data were substituted with the detection limit of a given element divided by the square root of 2. We conducted a PCA on the centred log ratio

(CLR)-transformed data in *R version 3.5.0* (R Core Team, 2019). We used the *CLR* function in the *R* package *compositions* to transform the data (Van Der Boogaart and Tolosana-Delgado, 2006), and the *PRCOMP* function in the statistical package to compute the PCA.

Mineral composition

Magnetite

Magnetite compositions ($n = 160$) were obtained from 18 samples comprising various types of metamorphosed altered rocks (i.e. garnet–biotite–quartz–cordierite±anthophyllite–gahnite rock (Dawson)), massive sulfides, and single samples of pink-banded unit (Horseshoe) and plagioclase–amphibole rock (El Plomo). In addition to the so-called spinel elements of Nadoll *et al.* (2012), which are Fe, Al, Ti, Mg, Mn, Zn, Cr, V, Ni, Co and Ga, the average, minimum and maximum concentrations of Si, Ca, Sn and Pb are reported in Table 3. Unless stated otherwise, comparisons of trace-element compositions are made for average compositions of magnetite. Bivariate plots are shown for Mg vs Al (Fig. 4a), Al vs Ti (Fig. 4b), V vs Mn (Fig. 4c), V vs Co (Fig. 4d), Ga vs Zn (Fig. 4e) and Zn vs Cu (Fig. 4f). There is a general increase in the Mg content of magnetite with Al, and there is a tendency for compositions from different locations to cluster in different areas in plots of Al vs Ti and V vs Mn. In particular, there is a distinct cluster in the average concentrations of Al

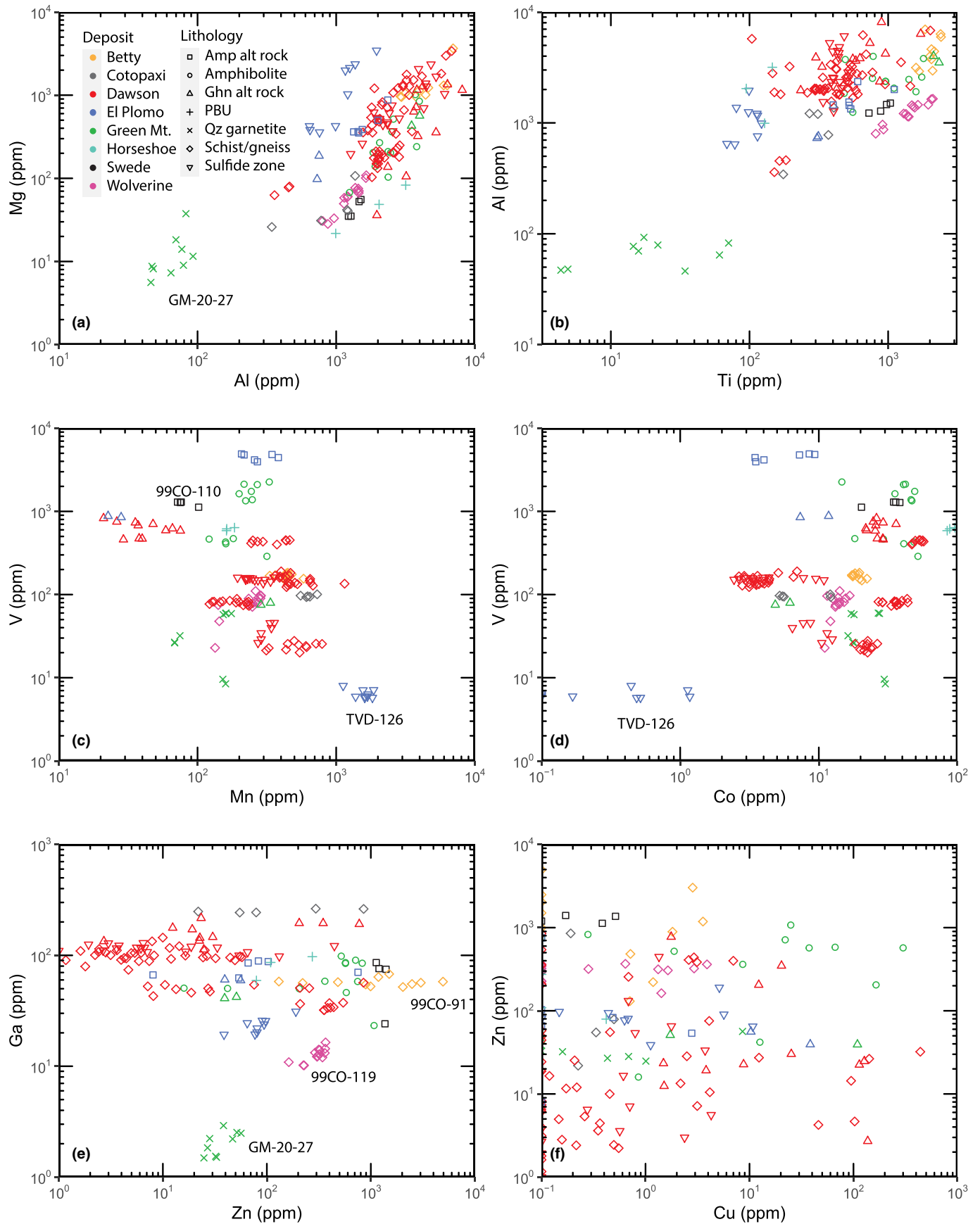


Figure 4. Bivariate trace-element plots (ppm) for magnetite ($n=160$) from the Betty, Cotopaxi, Dawson, El Plomo, Green Mountain, Horseshoe, Swede and Wolverine deposits. (a) Mg vs Al; (b) Al vs Ti; (c) V vs Mn; (d) V vs Co; (e) Ga vs Zn; and (f) Zn vs Cu.

Magnetite in samples (99CO-91) and (99CO-110) from these two deposits, respectively, also contains < 1 ppm Cu, which is among the lowest concentrations of Cu for samples studied here (Table 3). Magnetite in sample 99CO-91 also contains the highest average concentrations of Mg (1430 ppm), Al (5353 ppm), Ti (2030 ppm) and Sn (105.1 ppm).

Four of the six samples from the Dawson deposit (TVD-26, TVD-93, TVD-129, and TVD-131) are metamorphosed altered rocks that contain various combinations and amounts of quartz, cordierite, plagioclase and biotite (with or without the presence of sulfides). Magnetite in sample TVD-93 contains the highest average concentrations of Co (52 ppm), Ni (8.19 ppm), and Zn (386.7 ppm) in magnetite of the six Dawson samples, and it also contains the lowest concentrations of Al (2091 ppm), Ti (157.9), Ga (34.5 ppm), and Sn (0.26 ppm). The lowest concentrations of Cr (0.87 ppm), Co (3.86 ppm), Ni (0.14 ppm), Cu (0.18 ppm), Zn (8.29) and Pb (0.28 ppm) in Dawson samples occur in magnetite from sample TVD-129. The other two samples, TVD-26 and TVD-131, generally have elemental concentrations in magnetite that lie between the maximum and minimum concentrations of samples TVD-93 and TVD-128. Sample TVD-40B, a biotite–anthophyllite–gahnite rock, contains magnetite with the highest average concentrations of Al (4231 ppm), Si (1184 ppm), Ca (1074 ppm), Ti (710.1 ppm), V (626.6 ppm), Cr (37.9 ppm) and Ga (165.3 ppm) in samples from the Dawson deposit, as well as the lowest concentration of Mn (43.2 ppm).

Metamorphosed altered rocks in the El Plomo deposit contain more amphibole and less quartz than the samples analysed here from the Dawson deposit. These amphibole-bearing samples (TVD19-31 and TVD19-41) contain magnetite with lower average concentrations of Al (1688 and 741.2 ppm) and higher concentrations of V (4513 and 864.1 ppm) and Cr (73.1 and 965.8 ppm) than those from Dawson. Sample TVD19-41 contains magnetite with the highest concentration of Pb (357.2 ppm) of all samples. Magnetite in a sulfide-rich sample (TVD-126) from El Plomo, contains lower concentrations of Al (1110 ppm), Ti (98.7 ppm), V (6.42 ppm), Co (0.44 ppm) and Sn (0.68 ppm) relative to a sulfide-bearing sample (TVD-130) from Dawson (Al = 3114 ppm, Ti = 424.4 ppm, V = 116.1 ppm, Co = 6.3 ppm and Sn = 5.40 ppm).

The trace-element concentrations of magnetite in metamorphosed igneous rocks were also analysed. Magnetite in the pink banded unit from Horseshoe (TVD19-48) contains among the lowest amounts of Mg (51 ppm), Ca (6.47 ppm), Ti (123.1 ppm) and Cu (0.14 ppm) of any samples analysed while also containing among the highest concentrations of Cr (844.6 ppm), Co (89.3 ppm), Ni (368.4 ppm) and Pb (189.5 ppm). Magnetite in amphibolite (EHB-20-015 and AHCO-29) from the Green Mountain deposit contains among the highest concentrations of Ti (1500 ppm), Cr (2092 ppm), Cu (72.4 ppm) and Zn (640.1 ppm) (Fig. 4).

The PCA for magnetite includes Al, Ca, Co, Cr, Cu, Ga, Mg, Mn, Ni, Pb, Si, Sn, Ti, V and Zn. Principal component 1 represents 28.9% of the variance with V, Co and Cr correlating negatively with Mg, Mn and Sn (Fig. 5a,b). Principal component 2 accounts for 13.9% of the variance with Ni, Pb and Zn negatively correlating with Al, Ga and Ti (Fig. 5a,b). Magnetite compositions from El Plomo seen in Fig. 5a reflect the elevated concentrations of V, Cr and Co shown in Table 3 and Fig. 4c, whereas those for the Betty deposit cluster as a result of the high concentration of Mn. Similarly, a cluster of magnetite compositions from

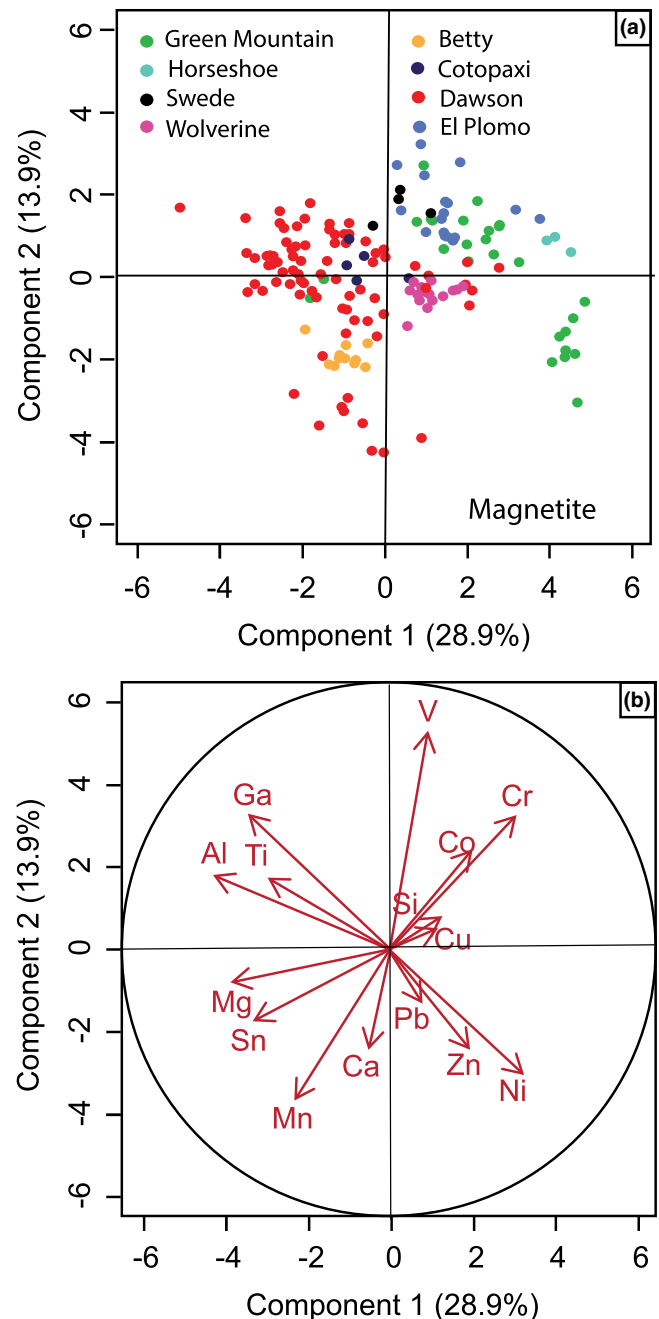


Figure 5. Principal component analysis of 15 elements (Al, Ca, Co, Cr, Cu, Ga, Mg, Mn, Ni, Pb, Si, Sn, Ti, V and Zn) in magnetite ($n = 160$) for all rocks studied here from the Colorado deposits. (a) Score plot of the first two principal components, with the percentage of variance for each component noted in parentheses. (b) Loading plot showing the geometric representation of how data were projected onto the score plot with respect to each element.

Dawson show component 2 scores < -2, which primarily reflects the Mn content, and a broad swath of other compositions from Dawson reflect elevated amounts of Ga, Al and Ti (Fig. 5b).

Ilmenite

In general, ilmenite contains a variety of compatible and incompatible trace elements including Cr, Hf, Mn, Nb, Ni, Ta, V, Zn and Zr (e.g. Charlier *et al.*, 2007; Jia *et al.*, 2022), with solid

solutions occurring among Fe, Mn, Mg and Zn. End-member eandrewsite (ZnTiO_3) and pyrophanite (MnTiO_3) together with solid solutions between them occur in altered rocks associated spatially with metamorphosed ore deposits (e.g. Birch *et al.*, 1988; Ghosh and Praveen, 2007; Tott *et al.*, 2019). The trace-element content of ilmenite was analysed here ($n = 82$) in samples of gahnite-bearing altered rocks (Green Mountain), gedrite–cordierite rocks (Evergreen), an anthophyllite–plagioclase rock (El Plomo), and a garnet-bearing amphibolite (Green Mountain) (Table 4). Although ilmenite and magnetite occur in the samples from Green Mountain and El Plomo, ilmenite is the only member of the system Fe–Ti–O present in samples from the Evergreen prospect.

Ilmenite compositions approach end-member FeTiO_3 , with up to 1.78 wt.% Mg and 1.29 wt.% Mn in samples from Green Mountain. Although ilmenite from Evergreen and El Plomo contains <2200 ppm Mn, sample 99CO-65B from Evergreen contains the highest Mn content (14218 ppm) (Fig. 5a). Moreover, this sample, along with the other sample from Evergreen (99CO-63), contains the highest concentrations of V (3048 and 2092 ppm, respectively) (Fig. 6a,c). Three of the seven samples from Green Mountain contain ilmenite in metamorphosed altered rocks, whereas sample AHCO-29 is an amphibolite. Compared to these other three samples, ilmenite in AHCO-29 contains the highest concentration of Al (241.8 ppm) and Cr (18.6 ppm) (Fig. 6d) along with Si (307.4 ppm), Ca (241.8 ppm), V (165.6 ppm) and Co (96.8 ppm), and the lowest amount of Nb (405.0), Sn (32.89 ppm), and Ta (118.0 ppm). Of the three base metals (Cu, Pb and Zn), the concentration of Zn in ilmenite is generally (but not always) an order of magnitude higher (100s to 1000s of ppm, with one exception of 10 ppm) than the concentration of Cu and Pb (<70 ppm), with single anomalous values of Cu (1058) and Pb (647.1 ppm) (Fig. 6b,e). Overall, ilmenite is elevated in Nb (137.4 to 2546 ppm) and Ta (47.2 to 875.0 ppm) relative to their contents in magnetite in which both elements are below the limits of detection (Fig. 6f). The ratio of Nb:Ta ranges from 1.52 to 3.43, with the highest value being for ilmenite in amphibolite from Green Mountain.

Amphibole

Amphiboles are characterised by a large number of crystallographic sites that accommodate a wide variety of major and trace elements (e.g. Schumacher, 2007). Although there are a plethora of major-element data in the literature (e.g. Leake, 1968; Gion *et al.*, 2022), there are few studies of the trace-element compositions of amphibole. Previous studies have focused on the trace-element composition of amphibole in igneous rocks with only a very limited number focusing on amphibole in metamorphic rocks (e.g. Skublov and Drugova, 2003; Mulrooney and Rivers, 2005). There are no previous studies on the trace-element compositions of amphibole associated spatially with metamorphosed massive sulfide deposits.

The major-element composition of amphibole (anthophyllite, actinolite, gedrite, cummingtonite and hornblende) associated spatially with 12 metamorphosed massive sulfide deposits in Colorado were previously obtained by Heimann (2002) and presented in $\text{MgO-Al}_2\text{O}_3\text{-FeO}$ ternary diagrams in Heimann *et al.* (2005). In addition, the composition of gedrite from Evergreen is given in Heimann *et al.* (2006). In this work, we obtained the major-element composition ($n = 148$) of amphibole from 19 samples of metamorphosed altered rocks (gedrite/anthophyllite–cordierite–gahnite rocks and anthophyllite–biotite rocks), and

massive to disseminated zones of sulfides from the Dawson, El Plomo, Green Mountain, Cinderella, Evergreen and Betty deposits (Table 5). They were collected to complement those obtained previously and to use the composition of Mn as an internal standard for LA-ICP-MS analyses. The amphiboles analysed here are gedrite, anthophyllite and hornblende. In addition to the major elements, Zn, F and Cl were also analysed by electron microprobe in several samples. The limited number of data obtained show that the clin amphiboles contain up to 0.36 wt.% ZnO, and up to 0.60 wt.% F, whereas ortho amphiboles contain up to 0.31 wt.% ZnO and 0.64 wt.% F. Concentrations of Cl were below detection limits for both structural varieties of amphibole.

Although LA-ICP-MS analyses were not standardised for the major elements (e.g. Mg, Al, Si and Fe), these elements for ortho amphibole and clin amphibole show percent level concentrations as expected (Tables 6 and 7). A notable feature of the trace-element concentrations of both ortho amphibole and clin amphibole is that they are variable within and between massive sulfide deposits (Figs 7 and 8). For example, ortho amphibole in metamorphosed altered rocks and sulfide zones from the Dawson deposit show the following compositional ranges: 33.4 to 232.3 ppm Li; 3.40 to 14.6 ppm B; 0 to 270 ppm P; 1.28 to 6.17 ppm Cr (Fig. 7a); 10.1 to 29.1 ppm Sc (Fig. 7b); 0 to 0.21 Ni; 0.33 to 52.5 ppm Co (Fig. 7c); 0.1 to 160.2 ppm Ga (Fig. 7e); 0.17 to 93.2 ppm Zr; and 0.41 to 144.8 ppm Sn (Fig. 7f). The highest values of V, Cr, Ni and Pb are for gedrite in a sulfide sample from El Plomo (TVD19-59). The base metals in ortho amphibole from Dawson contain as much as 1373 ppm Cu, 3159 ppm Zn and 15.1 ppm Pb (Fig. 7d–h). Higher average concentrations of Li (992.2 ppm), B (46.1 ppm), P (305.2 ppm), Sc (105.7 ppm, Fig. 7b), Ti (3720 ppm, Fig. 7b), Co (125.2 ppm), Zn (8440 ppm, Fig. 7d–h), Ga (542.0 ppm, Fig. 7e) and Zr (1810 ppm) occur in anthophyllite from the sulfide zone in the Cinderella deposit. Although amphibole analysed from the El Plomo, Cotopaxi and Betty deposits falls within the range of concentrations reported for amphibole from Dawson and Cinderella samples, one anomalous value of 927.4 ppm Pb in sample 99CO-89 from the Betty deposit was also obtained. It is probable that this is the result of ablation of a small inclusion of a Pb-bearing mineral; possibly galena. Ortho amphibole are generally depleted in REE, especially in gedrite where most values are at or below detection limits. However, three samples of anthophyllite (TVD-24, 99CO-3, 99CO-89) have concentrations of REE above detection limits for elements heavier than Eu (Table 6). In these three samples, the average concentrations in anthophyllite range from 0.64 to 14.4 ppm Gd, 2.46 to 50.4 ppm Dy, 2.13 to 60.9 ppm Er and 2.00 to 46.6 ppm Yb.

The PCA for ortho amphibole includes B, Ca, Co, Cr, Cu, Ga, Ge, K, Li, Na, Nb, P, Pb, Sc, Sn, Ti, V, Y, Zn and Zr. Principal component 1 (PCA1) represents 25.4% of the variance with principal component 2 (PCA2) accounting for 24.3% of the variance (Fig. 8a). Ortho amphibole for the five locations (Betty, Cinderella, Cotopaxi, Dawson and El Plomo), studied here cluster in different areas on the score plot of the first two principal components. The anthophyllite sample from the Cinderella deposit, which has score plots for PCA1 <0 and PCA2 >0 reflects the high concentrations of Ga, Li, Na, Nb, Sn and Zr (Fig. 8a,b; Table 6), whereas samples from El Plomo reflect elevated contents of Co, Cr and V, which are shown in the loading plot in the field marked by PCA1 and PCA2 having values < 0 (Fig. 8b). Ortho amphibole from Dawson are characterised by PCA2 scores >0 (excluding one outlier near 0 for PCA2) with data for others at Dawson reflecting

Table 4. Trace-element concentrations (in ppm) of ilmenite from LA-ICP-MS.

Rock type*		1	2	3	4	5	6	7	8
Sample		AHCO-25	AHCO-29	AHCO-35	TVD19-89	99CO-63	99CO-65B	TVD19-41	TVD19-48
<i>n</i>		34	4	20	2	10	8	3	6
Mg	Ave	15,844	3184	17,855	3610	2191	1159	515.7	284.8
	Max	24,326	3223	26,983	3628	4700	2251	949	349.6
	Min	10,853	3086	13,541	3592	326.9	827.1	216.9	226.2
Al	Ave	111.5	241.8	112.5	175.9	1538	215.7	435.8	1458
	Max	271.7	498.1	254.0	241.4	7993	348.7	734.8	2453
	Min	51.2	126.3	41.3	110.5	38.8	106.8	182.9	897.6
Si	Ave	239.0	307.4	254.6	150.4	703.3	231.9	583.8	236.1
	Max	1017	337.9	802.3	153.4	2888	471.1	1104	441.9
	Min	75.8	275.8	101.0	147.5	80.9	124.9	139.2	81.9
Ca	Ave	b.d.	241.8	b.d.	b.d.	b.d.	b.d.	1470	b.d.
	Max	281.0	932.3	622.8	19.6	105.0	116.5	3949	23.9
	Min	b.d.	b.d.	b.d.	b.d.	b.d.	b.d.	174.4	b.d.
Sc	Ave	43.5	66.0	35.6	610.2	43.2	119.7	80.6	174.9
	Max	59.9	75.1	67.3	668.3	64.2	255.7	90.5	229.4
	Min	32.8	57.4	16.3	552.0	29.0	73.4	74.6	119.6
Ti	Ave	374,306	864,852	432,874	461,582	471,789	805,897	339,173	106,933
	Max	546,320	914,651	543,279	461,845	511,507	848,631	372,959	115,265
	Min	269,461	806,532	366,460	461,318	435,782	775,638	296,826	98,350
V	Ave	7.33	165.6	16.1	9.87	2092	3048	1389	918.9
	Max	11.7	199.8	25.2	11.5	2189	3297	1556	992.5
	Min	4.84	115.8	9.30	8.26	1824	2775	1286	797.4
Cr	Ave	b.d.	18.6	b.d.	b.d.	73.3	54.6	1085	208.2
	Max	b.d.	27.5	b.d.	b.d.	83.1	72.7	1231	385.4
	Min	b.d.	9.16	b.d.	b.d.	62.8	38.8	913.8	55.1
Mn	Ave	10,375	12,681	12,992	10,801	2158	14,218	2968	2539
	Max	14,262	13,925	18,789	11,268	2505	19,548	3636	3554
	Min	6720	11,871	10,386	10,335	1782	12,114	2342	1958
Co	Ave	2.69	96.8	3.59	5.75	52.2	68.3	11.2	33.9
	Max	4.49	113.4	6.96	5.78	57.4	99.1	12.3	54.9
	Min	1.00	88.1	1.94	5.73	46.1	36.5	9.55	22.5
Cu	Ave	69.2	47.4	1058	54.4	29.1	5.40	29.6	8.95
	Max	244.1	56.8	4233	58.2	34.0	6.44	31.9	10.0
	Min	20.3	39.7	21.4	50.6	20.5	4.90	27.7	6.85
Zn	Ave	2479	664.6	3547	15.3	389.6	345.4	307.6	103.4
	Max	6818	862.7	10843	19.4	608.3	404.4	417.1	358.4
	Min	401.1	483.3	90.2	11.3	292.7	282.7	240.1	27.6
Ga	Ave	0.76	2.67	0.60	0.54	1.12	1.76	2.74	31.3
	Max	1.51	3.26	0.99	0.80	1.99	2.34	3.63	36.5
	Min	b.d.	1.68	b.d.	b.d.	0.66	1.05	1.89	27.2
Zr	Ave	7.09	3.53	47.3	3.27	6.63	5.72	0.67	28.2
	Max	13.1	5.69	690.1	4.22	12.3	11.3	1.36	55.6
	Min	1.14	2.54	1.91	2.31	1.90	1.91	0.31	9.36
Nb	Ave	969.5	405.0	2546	902.6	137.4	159.7	445.4	324.6
	Max	2271	560.2	3174	1341	167.4	226.5	511.4	482.7
	Min	152.4	266.8	913.7	463.9	111.5	135.8	378.5	224.0
In	Ave	0.46	0.64	0.32	7.29	0.72	1.40	0.15	1.19
	Max	1.35	0.80	0.71	7.78	1.02	1.71	0.19	1.46
	Min	0.14	0.52	0.09	6.81	0.36	1.01	0.09	0.92
Sn	Ave	51.4	32.9	63.5	120.9	37.5	55.7	51.3	311.8
	Max	154.5	35.0	120.2	127.3	41.9	62.7	74.2	389.3
	Min	17.8	28.1	24.5	114.6	31.1	51.9	36.4	249.1
Hf	Ave	1.00	b.d.	1.64	b.d.	0.49	0.87	b.d.	2.56
	Max	1.94	0.45	14.3	b.d.	1.18	2.00	b.d.	4.28
	Min	0.45	b.d.	b.d.	b.d.	b.d.	0.42	b.d.	0.81
Ta	Ave	636.4	118.0	875.0	469.8	47.2	57.1	253.3	189.4
	Max	1943	169.9	1085	529.8	54.1	92.2	286.1	233.8
	Min	20.2	47.8	139.4	409.7	40.6	37.1	227.9	148.5
Pb	Ave	15.6	10.6	51.7	1.07	4.07	1.14	7857	42.2
	Max	65.1	28.4	647.1	1.65	12.2	3.26	9888	212.3
	Min	b.d.	b.d.	2.84	b.d.	b.d.	b.d.	55.2	b.d.

Notes: *n* = number of analyses; mineral abbreviations after Warr (2021); Ave = average concentration; Max = maximum concentration; Min = minimum concentration; b.d. = below detection limit

*Key to rock type and deposit: 1 = gahnite-bearing altered rock (Green Mt.), 2 = amphibolite (Green Mt.), 3 = gahnite-bearing altered rock (Green Mt.), 4 = gahnite-bearing altered rock (Green Mt.), 5 = gahnite-free altered rock (Evergreen), 6 = gahnite-free altered rock (Evergreen), 7 = gahnite-free altered rock (El Plomo), 8 = pink banded unit (Horseshoe)

enrichments in the same elements shown for the Cinderella sample, whereas others reflect higher concentrations of Cu, P and Zn (Fig. 8a,b).

Although only three samples of clin amphibole (i.e. hornblende) were analysed, sample TVD19-96 of hornblende in a gahnite-bearing altered rock from Green Mountain and sample

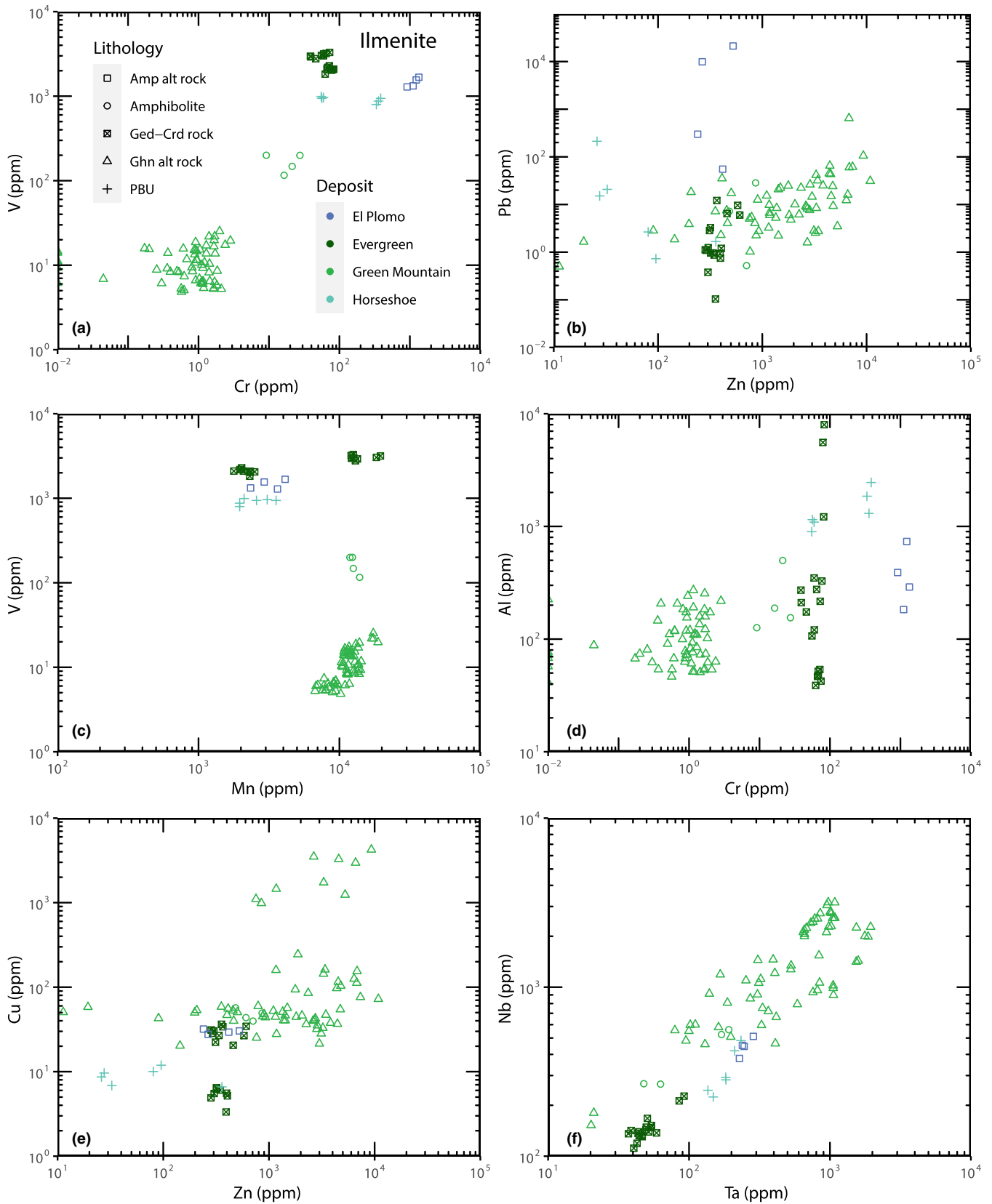


Figure 6. Bivariate trace-element plots (ppm) for ilmenite ($n=80$) from the El Plomo, Evergreen and Green Mountain deposits. (a) V vs Cr; (b) Pb vs Zn; (c) V vs Mn; (d) Al vs Ga; (e) Cu vs Zn; and (f) Nb vs Ta.

Table 5. Major-element compositions* of amphibole from central Colorado massive sulfide deposits.

Sample Deposit Mineral*	TVD-18 Dawson Ged <i>n</i> = 4	TVD-24 Dawson Ath <i>n</i> = 6	TVD-53 Dawson Ged <i>n</i> = 4	TVD-74 Dawson Ath <i>n</i> = 4	TVD19-25 El Plomo Hbl <i>n</i> = 9	TVD19-43 El Plomo Ath <i>n</i> = 17	TVD19-43 El Plomo Hbl <i>n</i> = 7	TVD19-59 El Plomo Ath <i>n</i> = 5	TVD19-60 El Plomo Ath <i>n</i> = 10	TVD19-60 El Plomo Hbl <i>n</i> = 15
Wt.%										
SiO ₂	47.78	57.45	48.03	51.52	44.31	47.21	43.33	47.87	47.98	42.93
TiO ₂	0.08	0.02	0.15	0.10	0.15	0.34	0.70	0.16	0.19	0.25
Al ₂ O ₃	29.27	2.45	10.56	7.30	9.16	10.13	13.12	8.26	8.62	13.19
FeO	6.20	6.36	13.79	12.62	14.49	18.69	13.34	20.62	20.43	14.46
MnO	0.41	0.15	0.74	0.92	0.73	0.66	0.30	0.54	0.56	0.23
MgO	13.62	30.63	21.65	23.84	14.14	18.84	14.08	18.24	18.25	13.10
CaO	0.14	0.56	0.38	0.59	11.02	0.66	10.29	0.65	0.61	10.36
Na ₂ O	0.63	0.31	1.24	0.83	1.46	1.31	1.80	1.05	1.04	1.63
K ₂ O	0.01	0.00	0.01	0.10	0.15	0.26	0.17	0.16	bd	0.75
ZnO	0.07	0.00	0.01	0.07	0.36	0.10	0.07	0.03	b.d.	b.d.
Cl	b.d.	b.d.	b.d.	b.d.	b.d.	b.d.	b.d.	b.d.		
F						0.32	0.40	0.25		
Total	98.21	97.94	96.57	97.91	96.97	98.52	97.58	97.83	97.67	96.90
Apfu										
Si	6.591	8.040	7.155	7.518	6.511	6.862	6.338	6.975	6.998	6.293
Ti	0.009	0.002	0.016	0.011	0.017	0.028	0.077	0.018	0.021	0.082
Al ^{IV}	1.409	0.000	0.845	0.482	1.489	1.138	1.662	1.147	1.002	1.707
Al ^{VI}	3.288	0.403	1.010	0.774	0.011	0.597	0.600	0.271	0.479	0.571
Fe	0.749	0.744	1.719	1.540	1.779	2.272	1.632	2.512	2.492	1.773
Mn	0.050	0.018	0.093	0.113	0.091	0.081	0.037	0.066	0.069	0.028
Mg	2.837	6.390	4.809	5.186	3.095	4.082	3.071	3.963	3.968	2.863
Ca	0.022	0.085	0.061	0.093	1.740	0.102	1.613	0.102	0.095	1.627
Na	0.179	0.085	0.357	0.235	0.417	0.370	0.509	0.296	0.295	0.464
K	0.001	0.001	0.001	0.002	0.067	0.001	0.032	0.001	b.d.	0.047
Zn	0.007	0.031	0.014	0.007	0.035	0.011	0.007	0.003	b.d.	b.d.
Cl	b.d.	b.d.	b.d.	b.d.	b.d.	b.d.	b.d.	b.d.		
F						0.151	0.198	0.123		
Sample Deposit Mineral*	TVD19-80 Green Mt. Ath <i>n</i> = 14	TVD19-88 El Plomo Ath <i>n</i> = 7	TVD19-96 Green Mt. Hbl <i>n</i> = 8	99CO-1 Cinderella Act <i>n</i> = 2	99CO-3 Cinderella Ath <i>n</i> = 2	99CO-12 Cotopaxi Ath <i>n</i> = 2	99CO-64B Evergreen Ged <i>n</i> = 13	99CO-65A Evergreen Ged <i>n</i> = 2	99CO-71 Cotopaxi Tr <i>n</i> = 9	99CO-89 Betty Ath <i>n</i> = 8
Wt.%										
SiO ₂	52.68	51.92	47.55	53.94	58.04	52.66	44.05	45.11	52.46	56.39
TiO ₂	bd	0.08	0.44	0.17	0.03	0.05	0.03	0.15	0.18	0.02
Al ₂ O ₃	2.08	5.63	8.42	4.05	1.27	3.97	13.76	12.57	5.30	1.10
FeO	19.83	13.92	13.60	7.01	6.64	15.11	24.01	24.12	2.39	13.05
MnO	0.33	0.42	0.45	1.73	1.58	3.91	0.35	0.32	0.80	0.53
MgO	21.24	24.04	15.69	19.02	30.42	20.98	13.21	13.21	22.35	25.34
CaO	0.67	0.81	9.85	11.83	0.56	0.44	0.50	0.41	12.82	0.49
Na ₂ O	0.39	0.86	1.21	0.38	0.11	0.47	1.25	1.26	0.86	0.15
K ₂ O	b.d.	b.d.	0.21	0.17	0.04	b.d.	0.15	0.15	0.18	0.02
ZnO	b.d.	b.d.	b.d.	0.19	0.15	0.31	0.02	0.04	0.04	0.26
Cl				b.d.	b.d.	b.d.	b.d.	b.d.	b.d.	b.d.
F				0.15	b.d.	0.33	0.37	0.21	0.60	0.64
Total	97.23	97.67	97.42	98.64	98.84	98.23	97.70	97.55	97.98	97.99
Apfu										
Si	7.595	7.354	6.532	8.075	8.076	7.858	6.771	7.020	7.613	8.214
Ti	bd	0.008	0.073	0.018	0.003	0.005	0.017	0.017	0.020	0.024
Al ^{IV}	0.405	0.646	1.468	0.000	0.000	0.142	1.229	0.980	0.387	0.000
Al ^{VI}	0.000	0.294	0.582	0.698	0.210	0.556	1.308	1.324	0.522	0.189
Fe	2.391	1.649	1.739	0.856	0.777	1.887	3.188	3.139	0.290	1.354
Mn	0.041	0.050	0.043	0.214	0.019	0.494	0.047	0.042	0.098	0.065
Mg	4.564	5.076	3.160	4.139	6.346	4.669	3.052	3.064	4.837	5.503
Ca	0.104	0.124	1.582	1.850	0.083	0.069	0.082	0.068	1.994	0.073
Na	0.108	0.235	0.502	0.109	0.029	0.142	0.334	0.379	0.243	0.042
K	b.d.	b.d.	0.051	0.035	0.010	b.d.	0.004	0.007	0.219	0.002
Zn	b.d.	b.d.	b.d.	0.044	0.015	0.034	0.003	0.014	0.004	0.025
Cl				b.d.	b.d.	b.d.	b.d.	b.d.	b.d.	b.d.
F				0.070	b.d.	0.166	0.186	0.102	0.279	0.294

*Analysed by electron microprobe. Mineral abbreviations after Warr (2021). *n* = number of analyses; Apfu = atoms per formula unit; b.d. = below detection limit.

TVD19-25 from the sulfide zone from El Plomo mostly have concentrations that fall within the range of those reported here for the orthoamphibole (Tables 6 and 7). However, hornblende in sample

TVD19-43 from the sulfide zone from the El Plomo deposit contains a higher average concentration of V (432.3 ppm, Fig. 9a), Sc (74.2 ppm, Fig. 9b, c), Ti (4811 ppm, Fig. 9b), Zr (30.6 ppm) and

Table 6. Compositions of orthoamphibole (in ppm) from LA-ICP-MS analysis.

Sample Deposit Amphibole Lithology <i>n</i>	TVD-18 Dawson Ged Ghn alt 5			TVD-18 Dawson Ath Ghn alt 7			TVD-24 Dawson Ath Amp alt 17			TVD-30 Dawson Ath Amp alt 12		
	Ave	Max	Min	Ave	Max	Min	Ave	Max	Min	Ave	Max	Min
Li	232.3	260.0	207.6	43.9	55.4	41.6	33.4	47.6	22.2	121.6	140.1	90.1
Be	b.d.	14.6	b.d.	b.d.	b.d.	b.d.	b.d.	b.d.	b.d.	b.d.	b.d.	b.d.
B	b.d.	b.d.	b.d.	b.d.	b.d.	b.d.	b.d.	b.d.	b.d.	b.d.	b.d.	b.d.
Na	5208	5716	4563	4355	5370	4866	2640	3058	1995	14106	15412	13575
Mg	271,403	273,576	266,286	42,666	51,387	48,901	192,324	205,761	184,185	122,990	133,031	117,281
Al	681,399	692,549	673,590	25,147	30,660	25,385	10,928	13,249	7421	75,039	81,273	71,030
Si	859,307	877,288	820,198	77,737	93,300	88,596	282,116	299,400	265,440	233,780	252,690	212,538
P	b.d.	b.d.	b.d.	b.d.	b.d.	b.d.	b.d.	b.d.	b.d.	b.d.	b.d.	b.d.
K	70.0	373.5	b.d.	b.d.	104.0	b.d.	b.d.	b.d.	153.5	b.d.	b.d.	62.4
Ca	1310	1711	927.7	b.d.	766.5	b.d.	3211	3871	2570	3670	4072	3390
Sc	27.5	37.0	20.9	20.4	53.9	15.8	10.1	11.3	8.99	17.5	25.5	15.8
Ti	101.4	409.9	b.d.	469.4	593.0	529.1	118.5	159.0	78.5	1694	1820	1574
V	b.d.	b.d.	b.d.	8.03	12.0	8.33	1.97	2.38	1.28	38.9	43.5	37.5
Cr	b.d.	b.d.	b.d.	b.d.	b.d.	b.d.	b.d.	b.d.	b.d.	b.d.	b.d.	b.d.
Fe	87,574	89,113	86,436	44,340	54,005	48,768	53,610	56,705	49,912	177,595	186,065	166,889
Co	3.25	3.92	2.65	b.d.	1.87	b.d.	b.d.	1.49	b.d.	5.28	6.10	4.42
Ni	b.d.	b.d.	b.d.	b.d.	b.d.	b.d.	b.d.	b.d.	b.d.	b.d.	b.d.	b.d.
Cu	b.d.	b.d.	b.d.	b.d.	b.d.	b.d.	24.2	222.7	b.d.	b.d.	11.7	b.d.
Zn	2025	2167	1757	302.2	491.4	306.6	2964	3159	2817	1293	1401	1194
Ga	160.2	166.8	153.8	11.6	16.2	12.1	4.45	5.45	3.25	47.7	55.6	43.8
Ge	b.d.	9.21	b.d.	b.d.	b.d.	b.d.	b.d.	b.d.	b.d.	b.d.	b.d.	b.d.
As	b.d.	b.d.	b.d.	b.d.	b.d.	b.d.	b.d.	b.d.	b.d.	b.d.	b.d.	b.d.
Se	b.d.	b.d.	b.d.	b.d.	b.d.	b.d.	b.d.	b.d.	b.d.	b.d.	b.d.	b.d.
Rb	1.16	5.78	b.d.	0.25	0.86	b.d.	b.d.	0.64	b.d.	b.d.	b.d.	b.d.
Sr	1.34	6.72	b.d.	0.44	0.75	0.34	b.d.	0.67	b.d.	2.34	2.83	2.04
Y	9.05	42.2	b.d.	7.58	9.49	7.80	12.6	15.3	9.7	30.5	51.8	25.5
Zr	93.2	98.1	b.d.	b.d.	1.06	0.70	1.92	6.86	b.d.	4.55	6.66	1.99
Nb	b.d.	1.14	b.d.	b.d.	b.d.	b.d.	0.36	0.55	b.d.	1.21	1.65	0.89
Cd	b.d.	b.d.	b.d.	b.d.	b.d.	b.d.	2.89	3.98	1.87	2.23	3.26	1.33
In	b.d.	b.d.	b.d.	0.42	0.60	0.42	0.36	0.47	0.29	5.21	5.55	4.63
Sn	b.d.	b.d.	b.d.	72.3	90.6	74.3	23.1	26.2	18.3	501.2	526.4	473.0
Sb	b.d.	b.d.	b.d.	b.d.	b.d.	b.d.	b.d.	b.d.	b.d.	b.d.	b.d.	b.d.
Cs	10.4	11.1	9.50	b.d.	b.d.	b.d.	b.d.	b.d.	b.d.	b.d.	b.d.	b.d.
Ba	4.92	24.50	b.d.	b.d.	b.d.	b.d.	b.d.	b.d.	b.d.	b.d.	b.d.	b.d.
La	b.d.	b.d.	b.d.	b.d.	b.d.	b.d.	b.d.	0.31	b.d.	b.d.	b.d.	b.d.
Ce	b.d.	0.19	b.d.	b.d.	b.d.	b.d.	0.26	1.84	b.d.	b.d.	0.18	b.d.
Pr	b.d.	b.d.	b.d.	b.d.	b.d.	b.d.	b.d.	0.24	b.d.	b.d.	b.d.	b.d.
Nd	b.d.	b.d.	b.d.	b.d.	b.d.	b.d.	b.d.	b.d.	b.d.	b.d.	0.88	b.d.
Sm	b.d.	b.d.	b.d.	b.d.	b.d.	b.d.	b.d.	b.d.	b.d.	b.d.	1.24	b.d.
Eu	b.d.	0.20	b.d.	b.d.	b.d.	b.d.	b.d.	b.d.	b.d.	0.32	0.42	0.28
Gd	b.d.	b.d.	b.d.	b.d.	b.d.	b.d.	b.d.	b.d.	b.d.	2.37	3.67	1.53
Tb	0.14	0.69	b.d.	b.d.	0.14	b.d.	0.17	0.24	b.d.	0.52	0.65	0.38
Dy	2.04	9.68	b.d.	0.87	1.25	0.98	1.69	2.46	0.95	4.75	5.59	3.60
Ho	0.36	1.66	b.d.	0.29	0.41	0.28	0.43	0.50	0.32	1.08	1.21	0.85
Er	1.26	5.75	b.d.	1.25	1.76	1.25	1.55	2.13	1.22	3.42	6.93	2.46
Tm	b.d.	0.53	b.d.	0.23	0.40	0.22	0.27	0.35	0.20	0.61	2.07	0.31
Yb	1.14	4.67	b.d.	1.84	3.31	1.65	2.00	2.52	1.29	3.11	3.85	2.46
Lu	b.d.	0.49	b.d.	0.34	0.69	0.24	0.32	0.49	0.19	0.79	3.98	0.42
Hf	1.98	5.64	b.d.	1.37	9.20	b.d.	b.d.	b.d.	b.d.	b.d.	0.59	b.d.
Ta	b.d.	0.11	b.d.	b.d.	b.d.	b.d.	b.d.	b.d.	b.d.	b.d.	0.22	b.d.
W	0.42	1.64	b.d.	b.d.	b.d.	b.d.	b.d.	b.d.	b.d.	b.d.	b.d.	b.d.
Pb	1.02	1.35	0.76	1.59	6.25	0.53	0.17	0.38	b.d.	8.9	15.1	6.5
Bi	b.d.	b.d.	b.d.	1.0	3.75	b.d.	b.d.	b.d.	b.d.	4.49	27.5	b.d.

(continued)

Pb (266.3 ppm, Fig. 9h) than gedrite in the same sample (Tables 6 and 7). In general, the Sn and Zn concentrations of hornblende are higher in the Green Mountain sample compared to those from El Plomo (Fig. 9c–h). The Ti, V and Cr contents of hornblende from Green Mountain are the highest of any amphibole analysed here. Though the average concentrations of REE in hornblende for elements heavier than Eu are within the range of concentrations for the orthoamphiboles,

all REE lighter than and including Eu are considerably higher (i.e. La = 4.45 to 14.7 ppm; Ce = 19.4 to 77.7 ppm; Pr = 3.16 to 13.0 ppm; Nd = 11.3 to 67.2 ppm; Sm = 2.04 to 21.9 ppm; and Eu = 3.67 to 5.65 ppm) than those in orthoamphiboles (Table 7). A plot of REE for hornblende shows a convex shape for the LREE, a positive or negative Eu anomaly, and a flat pattern for the heavy rare earth elements (HREE) (Fig. 10).

Table 6. (Continued.)

Sample Deposit Amphibole Lithology <i>n</i>	TVD-53 Dawson Ged Ghn alt 16			TVD-74 Dawson Ath Sulf zone 7			TVD19-43 El Plomo Ged Sulf zone 15			TVD-59 El Plomo Ath Sulf zone 16		
	Ave	Max	Min	Ave	Max	Min	Ave	Max	Min	Ave	Max	Min
Li	102.1	122.5	85.4	106.5	111.1	95.0	161.2	177.9	118.9	110.2	162.1	71.2
Be	b.d.	b.d.	b.d.	b.d.	b.d.	b.d.	b.d.	b.d.	b.d.	b.d.	b.d.	b.d.
B	b.d.	b.d.	b.d.	b.d.	b.d.	b.d.	b.d.	b.d.	b.d.	b.d.	b.d.	b.d.
Na	8705	10,077	7725	6555	7383	5656	11,104	11,692	10,326	6933	8836	4382
Mg	132,737	139,899	122,345	146,254	154,825	137,449	127,694	129,561	122,019	114,721	123,991	104,903
Al	45,971	53,543	41,840	36,448	45,018	30,879	56,671	60,470	50,590	35,926	47,477	24,149
Si	226,409	236,378	198,027	264,375	278,829	244,943	250,366	267,228	234,858	257,880	280,408	244,070
P	b.d.	b.d.	b.d.	b.d.	b.d.	b.d.	b.d.	b.d.	b.d.	b.d.	b.d.	b.d.
K	b.d.	b.d.	b.d.	72.0	181.6	b.d.	b.d.	101.6	b.d.	90.7	226.5	b.d.
Ca	2275	2474	2128	3993	5020	3582	5515	7148	4008	3425	5803	3029
Sc	13.1	15.0	11.4	24.9	30.7	21.0	37.0	43.4	29.4	111.9	134.0	90.9
Ti	798.3	917.4	679.1	643.1	711.1	601.8	2123	2808	1196	1089	1372	511.1
V	13.4	14.9	11.4	41.6	49.7	37.1	277.0	291.4	258.3	423.4	528.0	362.3
Cr	b.d.	b.d.	b.d.	b.d.	b.d.	b.d.	733.8	946.0	522.2	776.3	990.4	631.4
Fe	112,831.9	117,116	104,473	136,071	174,211	109,324	169,057	176,715	159,848	180,558	195,793	168,031
Co	3.27	3.94	2.66	2.50	3.03	2.23	52.5	57.2	48.3	61.0	64.0	57.1
Ni	b.d.	b.d.	b.d.	b.d.	b.d.	b.d.	86.9	100.0	73.2	102.6	122.1	79.9
Cu	67.9	170.5	b.d.	304	1373	b.d.	b.d.	b.d.	b.d.	b.d.	b.d.	b.d.
Zn	1400	1744	1121	1702	2292	1470	1488	1745	1234	814.7	904.2	724.6
Ga	20.4	24.8	18.4	15.3	17.9	14.2	21.6	23.3	18.8	22.1	27.5	15.9
Ge	b.d.	b.d.	b.d.	b.d.	b.d.	b.d.	b.d.	b.d.	b.d.	b.d.	b.d.	b.d.
As	b.d.	b.d.	b.d.	b.d.	b.d.	b.d.	b.d.	5.33	b.d.	3.05	8.82	b.d.
Se	b.d.	b.d.	b.d.	b.d.	105.4	b.d.	b.d.	b.d.	b.d.	b.d.	b.d.	b.d.
Rb	b.d.	b.d.	b.d.	b.d.	b.d.	b.d.	b.d.	b.d.	b.d.	b.d.	2.53	b.d.
Sr	0.62	1.10	b.d.	1.31	2.43	0.62	1.15	1.68	0.56	1.62	4.59	0.57
Y	25.4	29.1	21.5	88.1	110.2	77.1	5.39	6.79	3.44	64.2	79.9	45.7
Zr	4.70	6.32	3.13	4.66	6.15	2.73	12.2	80.7	4.24	4.04	6.02	2.04
Nb	7.36	9.80	4.89	1.08	1.43	0.80	0.53	0.85	b.d.	0.41	0.77	b.d.
Cd	b.d.	1.76	b.d.	2.18	4.21	b.d.	1.27	2.20	b.d.	b.d.	1.89	b.d.
In	2.03	2.64	1.58	1.52	2.37	1.16	0.19	0.28	b.d.	0.29	0.34	0.21
Sn	135.3	167.4	107.2	144.8	176.8	132.7	4.81	5.68	b.d.	10.1	12.0	7.53
Sb	b.d.	b.d.	b.d.	b.d.	b.d.	b.d.	b.d.	6.13	b.d.	1.43	8.87	b.d.
Cs	b.d.	b.d.	b.d.	b.d.	b.d.	b.d.	b.d.	b.d.	b.d.	b.d.	b.d.	b.d.
Ba	b.d.	b.d.	b.d.	b.d.	4.67	b.d.	b.d.	b.d.	b.d.	b.d.	8.82	b.d.
La	b.d.	b.d.	b.d.	b.d.	b.d.	b.d.	b.d.	b.d.	b.d.	b.d.	1.02	b.d.
Ce	b.d.	b.d.	b.d.	0.31	0.88	b.d.	0.26	0.61	b.d.	0.47	3.02	0.40
Pr	b.d.	b.d.	b.d.	b.d.	0.14	b.d.	b.d.	b.d.	b.d.	b.d.	0.22	b.d.
Nd	b.d.	b.d.	b.d.	b.d.	1.22	b.d.	b.d.	b.d.	b.d.	b.d.	1.03	b.d.
Sm	b.d.	b.d.	b.d.	1.02	1.83	b.d.	b.d.	b.d.	b.d.	1.14	2.05	b.d.
Eu	0.20	0.39	b.d.	0.49	0.56	b.d.	b.d.	b.d.	b.d.	0.29	0.52	b.d.
Gd	2.30	3.63	1.66	4.12	4.86	3.38	b.d.	b.d.	b.d.	3.74	5.18	1.76
Tb	0.52	0.61	0.36	1.53	1.67	1.31	b.d.	b.d.	b.d.	0.99	1.24	0.60
Dy	4.12	4.92	3.31	14.1	18.2	11.8	0.73	1.23	0.38	9.13	11.5	6.72
Ho	0.90	1.10	0.72	3.17	3.88	2.60	0.18	0.30	0.08	2.26	3.06	1.62
Er	2.77	3.42	1.92	10.7	12.7	8.70	0.64	1.16	0.41	7.37	9.92	5.14
Tm	0.40	0.52	0.31	1.62	1.98	1.40	b.d.	0.15	b.d.	1.17	1.50	0.84
Yb	2.64	3.49	1.68	10.7	11.7	9.8	0.93	1.47	b.d.	8.04	10.6	6.15
Lu	0.42	0.52	0.30	1.61	1.82	1.43	0.18	0.23	b.d.	1.24	1.57	0.84
Hf	b.d.	0.52	b.d.	b.d.	0.68	b.d.	0.57	2.46	b.d.	0.47	1.78	b.d.
Ta	0.78	1.12	0.47	0.21	0.28	b.d.	b.d.	b.d.	b.d.	b.d.	b.d.	b.d.
W	b.d.	b.d.	b.d.	b.d.	0.47	b.d.	b.d.	2.83	b.d.	b.d.	0.53	b.d.
Pb	b.d.	0.41	b.d.	6.98	8.06	2.70	164.9	28.7	10.9	496.5	3131	6.97
Bi	0.45	1.31	b.d.	0.66	1.24	b.d.	b.d.	b.d.	b.d.	0.82	6.28	b.d.

(continued)

Discussion

Origin of magnetite and ilmenite

The elements Mg, Ti and Al are known to be mobile in high-temperature deuteric fluids but are generally immobile in low-temperature hydrothermal, and in some cases, metamorphic fluids (e.g. Nielsen *et al.*, 1994; Verlaquet *et al.*, 2006; Dare

et al., 2012, 2014; Magfour *et al.*, 2021). Nadoll *et al.* (2014) proposed that a plot of Al + Mn vs Ti + V of magnetite compositions is a useful indicator of the temperature of the original ore-forming fluid. Values of Ti + V of >1000 ppm are typically characteristic of fluid temperatures of ~300 to 500°C (high-temperature), whereas values <1000 ppm are more characteristic of fluid temperatures <300°C. Fluid temperatures between 200 and 300°C (medium

Table 6. (Continued.)

Sample Deposit Amphibole Lithology <i>n</i>	99CO-3 Cinderella Ath Ghn alt			99CO-12 Cotopaxi Ath Ghn alt			99CO-89 Betty Ath Ghn alt		
	Ave	Max	Min	Ave	Max	Min	Ave	Max	Min
Li	992.2	1208	608.1	25.9	42.5	11.6	5.86	14.9	2.64
Be	21.2	58.9	b.d.	b.d.	b.d.	b.d.	b.d.	b.d.	b.d.
B	46.1	126.6	b.d.	b.d.	b.d.	b.d.	b.d.	b.d.	b.d.
Na	92,452	96,342	72,941	4298	4986	3297	1442	1704	1084
Mg	560,369	857,781	462,039	144,325	159,598	132,249	181,881	201,810	158,981
Al	545,250	648,069	353,087	20,003	27,111	14,353	3998	4841	2783
Si	1,413,564	1,886,071	1,203,918	310,446	324,997	284,737	321,253	345,708	296,077
P	b.d.	835.5	b.d.	b.d.	b.d.	b.d.	b.d.	607.7	b.d.
K	454.4	2076	143.0	b.d.	54.9	b.d.	55.5	379.9	b.d.
Ca	22,498	37,542	19,626	3650	4261	2862	3923	5387	3032
Sc	105.7	139.0	62.9	41.1	44.8	38.4	16.3	18.8	13.1
Ti	3720	5210	2907	378.5	710.7	265.3	216.6	291.5	121.0
V	29.1	44.8	16.8	35.6	45.0	31.1	1.91	2.95	1.31
Cr	b.d.	b.d.	b.d.	b.d.	b.d.	b.d.	b.d.	b.d.	b.d.
Fe	1,435,032	1,878,452	1,152,459	149,788	166,424	141,102	144,649	153,786	132,751
Co	125.2	173.6	93.9	4.36	5.36	3.77	3.94	5.04	2.90
Ni	b.d.	b.d.	b.d.	b.d.	b.d.	b.d.	b.d.	b.d.	b.d.
Cu	802.8	3113	b.d.	71	232.5	b.d.	b.d.	12.4	b.d.
Zn	8440	15,770	5867	2713	4269	1665	2292	3128	1520
Ga	542.0	665.9	406.5	12.63	15.3	10.2	1.23	1.72	0.74
Ge	b.d.	12.5	b.d.	b.d.	b.d.	b.d.	b.d.	b.d.	b.d.
As	b.d.	8.71	b.d.	b.d.	b.d.	b.d.	b.d.	b.d.	b.d.
Se	b.d.	b.d.	b.d.	b.d.	b.d.	b.d.	b.d.	b.d.	b.d.
Rb	2.00	13.8	b.d.	4.13	28.7	b.d.	b.d.	3.11	b.d.
Sr	27.6	44.9	16.8	0.48	1.07	b.d.	0.92	3.11	b.d.
Y	297.9	393.8	175.3	58.2	68.7	45.2	66.2	84.1	45.8
Zr	1810	7870	15.9	4.44	25.7	1.48	2.02	14.3	0.44
Nb	41.5	54.9	32.2	0.77	2.03	b.d.	0.47	0.99	b.d.
Cd	4.47	8.17	b.d.	b.d.	b.d.	b.d.	b.d.	4.77	b.d.
In	4.52	5.55	3.69	b.d.	b.d.	b.d.	b.d.	b.d.	b.d.
Sn	83.5	108.0	51.7	2.86	3.48	1.91	b.d.	1.93	b.d.
Sb	6.92	52.0	b.d.	b.d.	b.d.	b.d.	b.d.	1.22	b.d.
Cs	1.18	5.86	b.d.	b.d.	1.51	b.d.	b.d.	0.38	b.d.
Ba	4.27	26.8	b.d.	12	79.3	b.d.	b.d.	1.29	b.d.
La	2.21	14.9	b.d.	b.d.	b.d.	b.d.	b.d.	0.86	b.d.
Ce	5.08	26.4	b.d.	b.d.	0.33	b.d.	0.47	3.29	b.d.
Pr	0.55	3.70	b.d.	b.d.	b.d.	b.d.	b.d.	0.34	b.d.
Nd	2.37	16.8	b.d.	b.d.	b.d.	b.d.	b.d.	2.43	b.d.
Sm	1.56	5.49	b.d.	b.d.	1.43	b.d.	b.d.	1.40	b.d.
Eu	0.86	1.76	b.d.	b.d.	0.23	b.d.	b.d.	b.d.	b.d.
Gd	14.4	22.8	9.40	2.80	4.93	1.48	2.54	3.80	1.04
Tb	5.29	7.34	3.51	0.85	1.25	0.39	0.85	1.04	0.56
Dy	50.4	70.9	35.1	7.97	10.6	5.02	7.82	9.65	4.93
Ho	12.4	17.8	5.19	1.93	2.67	1.03	2.36	3.33	1.52
Er	41.8	60.9	12.9	7.32	9.45	4.05	8.35	11.7	5.53
Tm	6.57	9.93	2.21	1.22	1.62	0.57	1.37	1.85	1.07
Yb	46.6	71.2	13.2	9.1	11.3	6.59	9.61	12.0	6.29
Lu	7.57	12.7	2.16	1.71	2.34	1.23	1.70	2.16	1.23
Hf	51.3	219.3	b.d.	0.67	5.41	b.d.	b.d.	0.64	b.d.
Ta	2.52	3.54	1.69	b.d.	0.12	b.d.	b.d.	b.d.	b.d.
W	b.d.	1.08	b.d.	b.d.	b.d.	b.d.	b.d.	0.38	b.d.
Pb	34.6	86.3	20.2	3.47	11.7	1.59	56.2	115.2	b.d.
Bi	0.23	1.44	b.d.	b.d.	b.d.	b.d.	7.50	10.2	b.d.

*Mineral abbreviations after Warr (2021); Ged – Gedrite; Ath – anthophyllite; Hbl – hornblende; Act – actinolite; Tr – tremolite; alt = altered; sulf = sulfide. *n* = number of analyses; Ave = average concentration; Max = maximum concentration; Min = minimum concentration; b.d. = below detection limit.

temperature) typically possess values of Al + Mn of ~350 to 7000 ppm, whereas those < ~200°C (low temperatures) have Al + Mn < ~350 ppm. Magnetite in altered rocks and sulfides from the Colorado deposits have values of Al + Mn = 198 to 5652 ppm and Ti + V = 65 to 5330 ppm with 14 of 18 samples of magnetite having ranges of Al + Mn and Ti + V of 197 to

4059 ppm and 402 to 2208 ppm, respectively. This suggests that the ore-forming fluids overlap the medium and higher temperature regimes (Fig. 11), consistent with the ore-forming fluid temperatures of ~270–350°C proposed by Berke *et al.* (2023), which were based on the stability of members in the system Cu–Fe–S–O (i.e. magnetite, chalcopyrite, pyrite and pyrrhotite), and isotope

Table 7. Trace-element compositions (in ppm) of calcic amphibole from LA-ICP-MS analysis.

n	TVD19-25 El Plomo Sulfide zone			TVD19-43 El Plomo Sulfide zone			TVD19-96 Green Mt. Ghn altered rock		
	12 Ave	Max	Min	13 Ave	Max	Min	13 Ave	Max	Min
Li	6.99	10.3	3.99	28.4	33.9	24.0	b.d.	2.73	b.d.
Be	b.d.	7.48	b.d.	b.d.	b.d.	b.d.	b.d.	9.00	b.d.
B	b.d.	b.d.	b.d.	b.d.	b.d.	b.d.	b.d.	b.d.	b.d.
P	b.d.	b.d.	b.d.	563	3999	b.d.	b.d.	b.d.	b.d.
K	2097	7346	909.2	1582	1876	1443	1491	1876	124.5
Sc	11.0	14.6	7.24	74.2	81.9	64.0	28.3	42.1	9.00
Ti	585.6	1398.7	308.4	4810	5454	4341	3608	5679	697.8
V	33.5	48.9	22.9	432.2	483.6	390.2	18.9	28.8	4.03
Cr	b.d.	b.d.	b.d.	860.6	1384	763.8	b.d.	b.d.	b.d.
Co	2.82	4.13	b.d.	39.8	43.2	35.0	8.71	11.7	5.61
Ni	b.d.	b.d.	b.d.	74.9	95.8	55.3	b.d.	b.d.	b.d.
Cu	b.d.	b.d.	b.d.	b.d.	b.d.	b.d.	b.d.	48.4	b.d.
Zn	1121	1415	424.2	822.1	934.3	713.6	1810	2215	1066
Ga	19.7	39.7	12.2	24.8	27.9	23.2	9.42	15.7	2.01
Ge	b.d.	b.d.	b.d.	b.d.	b.d.	b.d.	b.d.	b.d.	b.d.
As	b.d.	b.d.	b.d.	6.84	10.70	b.d.	b.d.	b.d.	b.d.
Rb	0.82	2.54	b.d.	b.d.	2.22	b.d.	b.d.	1.04	b.d.
Sr	11.4	26.7	3.67	8.20	18.9	6.23	15.8	26.0	1.41
Y	17.1	46.5	5.15	52.6	60.7	46.8	147.7	228.0	16.1
Zr	11.9	31.1	b.d.	30.6	58.4	24.4	37.0	152.9	1.84
Nb	3.36	10.4	1.23	2.33	3.55	1.52	21.0	32.3	2.55
Cd	b.d.	1.45	b.d.	3.34	4.79	2.84	4.50	9.12	1.69
Sn	18.3	52.4	5.96	12.6	14.5	11.7	66.4	110.8	10.9
La	4.45	7.48	0.13	14.5	19.8	11.8	12.1	23.3	0.77
Ce	19.4	33.3	1.87	57.1	68.1	49.8	77.7	122.8	4.71
Pr	3.16	5.19	0.39	7.76	8.67	7.20	13.0	21.3	0.77
Nd	11.3	18.0	4.61	34.9	37.5	29.0	67.2	106.6	3.47
Sm	2.04	3.03	1.20	9.10	9.03	7.82	21.9	38.8	1.06
Eu	3.67	6.00	2.17	5.65	6.30	4.94	4.61	7.58	0.32
Gd	2.33	4.81	b.d.	9.42	11.5	7.65	23.9	40.1	1.80
Tb	0.34	0.71	b.d.	1.46	1.70	1.29	4.12	6.58	0.34
Dy	2.88	8.23	0.72	9.91	11.3	8.43	26.4	43.3	2.11
Ho	0.56	1.56	0.18	1.81	2.00	1.46	4.86	7.54	0.51
Er	1.56	4.58	0.60	5.12	6.07	4.38	14.2	22.1	1.60
Tm	0.20	0.42	b.d.	0.72	0.84	0.59	1.99	3.25	0.25
Yb	1.38	2.68	0.82	4.87	5.83	3.74	13.4	20.4	1.97
Lu	0.22	0.55	b.d.	0.59	0.74	0.39	1.87	2.91	0.26
Hf	0.49	5.91	b.d.	1.17	1.99	0.86	2.17	4.47	1.13
Pb	32.2	41.9	21.8	266.3	775.1	149.6	151.1	282.1	16.6
Bi	b.d.	0.58	b.d.	b.d.	0.34	0.05	3.47	7.68	0.35

Note: n = number of analyses; Ave = average concentration; Max = maximum concentration; Min = minimum concentration; b.d. = below detection limit.

compositions of sulfides in the deposits. Of note is sample GM-20-027, which is a quartz garnetite from Green Mountain that was interpreted to be an exhalative rock by Berke *et al.* (2023). It has the lowest average concentrations of Al + Mn (198 ppm) and Ti + V (65 ppm) in magnetite of any sample analysed here and falls within the low-temperature field of Nadoll *et al.* (2014) and Maghfouri *et al.* (2021). Exhalative rocks are generally distal to the moderate- to high-temperature hydrothermal vent of VMS deposits and commonly form at lower temperatures (e.g. Spry *et al.*, 2000).

Various discrimination diagrams have been proposed in the literature to distinguish magmatic magnetite from hydrothermal magnetite. These include plots of Sn vs Ti (Pisiak *et al.*, 2015), V/Ti vs Fe (Wen *et al.*, 2017), Ti vs Ni/Cr (Dare *et al.*, 2014), Ti vs V (Nadoll *et al.*, 2014; Knipping *et al.*, 2015) and Al vs Ti (Canil *et al.*, 2016). In a plot of Sn vs Ti (Fig. 12a), for example, magnetite in massive sulfide deposits in Colorado suggests that the magnetite was in equilibrium with the ore-forming fluid and had a hydrothermal origin, whereas magnetite compositions

plotted in terms of Ti vs Ni/Cr occur in both the hydrothermal and magmatic fields (Fig. 12b). The utilisation of this diagram as a discriminator between a hydrothermal and igneous origin for magnetite is questionable given the caution raised by Pisiak *et al.* (2015) and Frank *et al.* (2022) that magnetite compositions from porphyry copper deposits cover both the igneous and hydrothermal fields.

Nadoll *et al.* (2014) proposed that igneous magnetite was enriched in Ti, with values > ~5000 ppm being characteristic. Although no sample from the Colorado deposits contain >5000 ppm it should be noted that ilmenite was exsolved from magnetite in some samples at Green Mountain and traces of hematite were exsolved from ilmenite at Evergreen. This raises the possibility that the ore-forming fluid was enriched in Ti and that magnetite might have had a magmatic origin (Fig. 3g). However, recent studies of titanomagnetite by Hu *et al.* (2022) show that high-Ti magnetite can be present in hydrothermal deposits and that exsolution between coexisting magnetite and ilmenite need not necessarily imply that they were the products

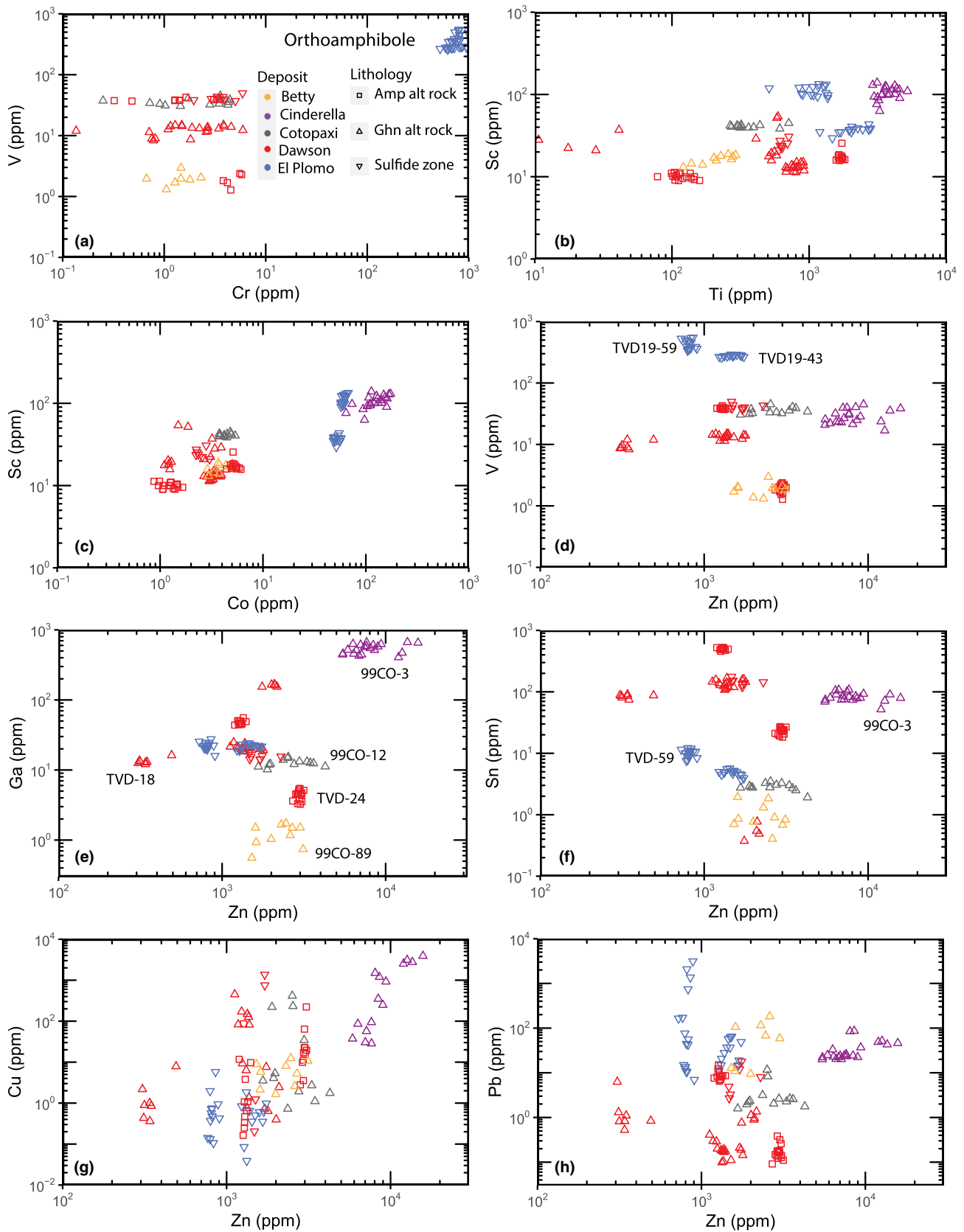


Figure 7. Bivariate trace-element plots (ppm) for orthoamphibole (anthophyllite and gedrite, $n = 139$) from the Betty, Cinderella, Cotopaxi, Dawson and El Plomo deposits. (a) V vs Cr; (b) Sc vs Ti; (c) Sc vs Co; (d) V vs Zn; (e) Ga vs Zn; (f) Sn vs Zn; (g) Cu vs Zn; and (h) Pb vs Zn.

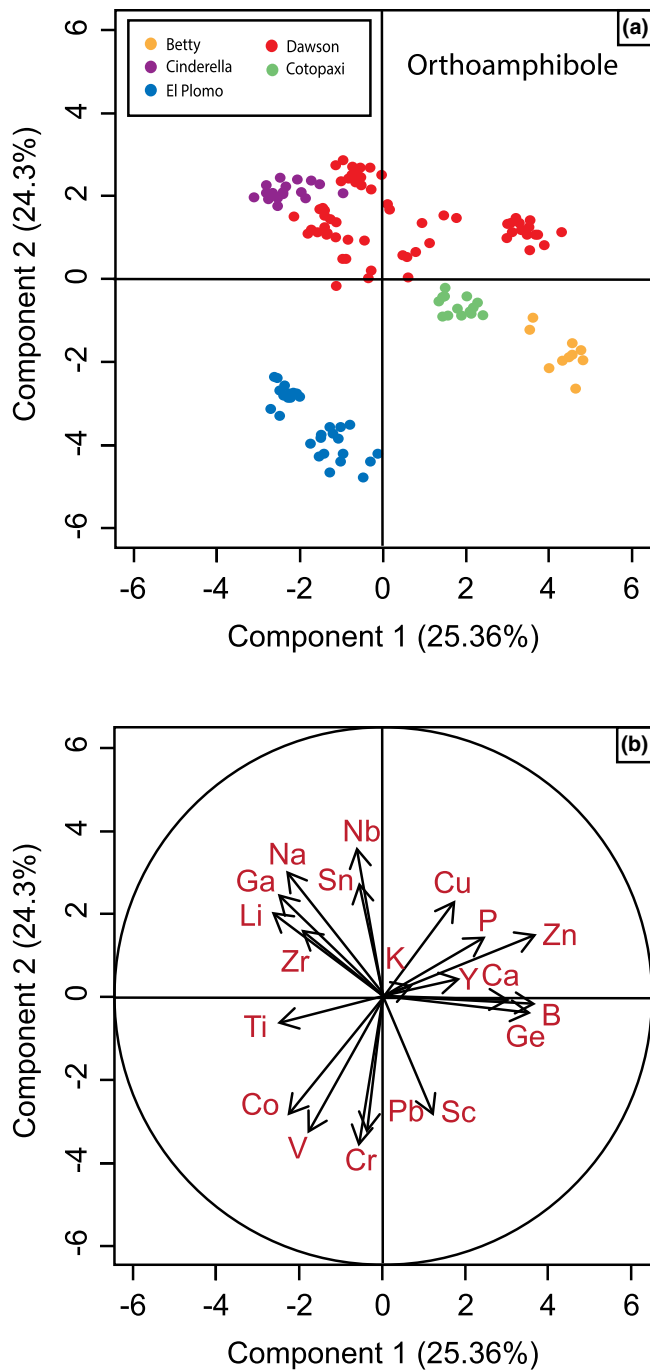


Figure 8. Principal component analysis of 20 elements (B, Ca, Co, Cr, Cu, Ga, Ge, K, Li, Na, Nb, P, Pb, Sc, Sn, Ti, V, Y, Zn and Zr) in orthoamphibole ($n=139$) from the Colorado deposits. (a) Score plot of the first two principal components, with the percentage of variance for each component noted in parentheses. (b) Loading plot showing the geometric representation of how data were projected onto the score plot with respect to each element.

of precipitation from a high-temperature magmatic fluid as was proposed previously by, for example, Knipping *et al.* (2015) and La Cruz *et al.* (2020).

In a study of the composition of magnetite in 15 metamorphosed VMS deposit subtypes, Makvandi *et al.* (2016a) identified three types of magnetite: magmatic, hydrothermal and metamorphic. Some of the magnetite evaluated by Makvandi *et al.* (2016a) was magmatic or hydrothermal with a metamorphic

(amphibolite facies) overprint. Unlike the examples shown by Makvandi *et al.* (2016a), those from Colorado showed no textural or compositional evidence for metamorphic overgrowths of magnetite on preexisting hydrothermal grains. Instead our petrographic studies suggest that magnetite in the metamorphosed altered rocks has a metamorphic origin because it contains inclusions of sulfides and silicates. Similar inclusions were identified by Makvandi *et al.* (2016a) and Sun *et al.* (2022) in metamorphic magnetite from the regionally metamorphosed Izok Lake Zn–Pb–Cu–Ag and Keketal Pb–Zn VMS deposits, respectively. Moreover, magnetite in the Colorado deposits is intergrown with orthoamphibole and gahnite, which are both metamorphic minerals. However, given that magnetite is also intergrown with pyrite and pyrrhotite suggests that magnetite initially formed under hydrothermal conditions. It is possible that magnetite and ilmenite in the metamorphosed altered rocks and the semi-massive to massive sulfides precipitated from this hydrothermal fluid and were subsequently recrystallised and metamorphosed while remaining in equilibrium with pyrrhotite and pyrite in sulfide samples. In contrast, magnetite in metamorphosed felsic (e.g. pink banded unit (PBU) sample) and mafic (e.g. amphibolite) igneous rocks probably formed from magmatic processes and were subsequently metamorphosed. The concentration of magnetite in the PBU sample occurs in an isolated part of the PCA (Fig. 5), where principal components 1 and 2 are both > 0 reflecting high concentrations of V and Cr. This sample also has the highest average concentrations of Ni (368 ppm). Similarly, magnetite in amphibolite from Green Mountain also has among the highest concentrations of V and Cr (although depleted in Ni) supporting the idea that the composition of magnetite in the igneous rocks reflect bulk compositional differences between the igneous rocks and altered (gahnite- and/or amphibole-bearing) and unaltered sedimentary/volcaniclastic rocks. It is probable that the most important parameter to explain the wide range in compositions in trace-element compositions of magnetite in the altered rocks is the variable degree to which the hydrothermal fluid has interacted with the host rocks of different compositions.

Ilmenite is present as an accessory phase in all of the rocks investigated and is most common in gahnite-bearing and gahnite-absent altered rocks. In these, ilmenite has a metamorphic origin given its intergrowth with other metamorphic minerals including anthophyllite, gahnite and cordierite. Although found in metamorphic rocks, ilmenite in amphibolite and the pink banded unit might have had an igneous precursor and been metamorphosed subsequently. Of note are the remarkably uniform Nb/Ta ratios of magnetite of 1.52 to 3.43 in the rocks studied regardless of the host-rock composition. Whether such low ratios are indicative of a metamorphic origin is unclear. However, note that ilmenite in igneous rocks (i.e. kimberlites) in the Kimberley diamond mine, South Africa have higher ratios (~ 5 to 37, Ene, 2014). Higher Nb/Ta ratios also occur in ilmenite (5 to 11) in kimberlite from the Monastery kimberlite, South Africa (Moore *et al.*, 1992) and in intrusive rocks (14.8 to 21.0) of the Skaergaard intrusion, Greenland (Jang and Naslund, 2003). Ilmenite with the highest Nb/Ta ratio in rocks investigated here (3.43) was from amphibolite. Although processes related to the crystallisation mechanism is considered to be an important factor controlling the composition of ilmenite, the nature of coexisting minerals also appears to be important. In the Colorado samples, those samples that contain gahnite in the metamorphosed altered rocks have higher average concentrations of Mg (3184 to 17855 ppm), Cu (17.4 to 1058 ppm) and Nb (405.0

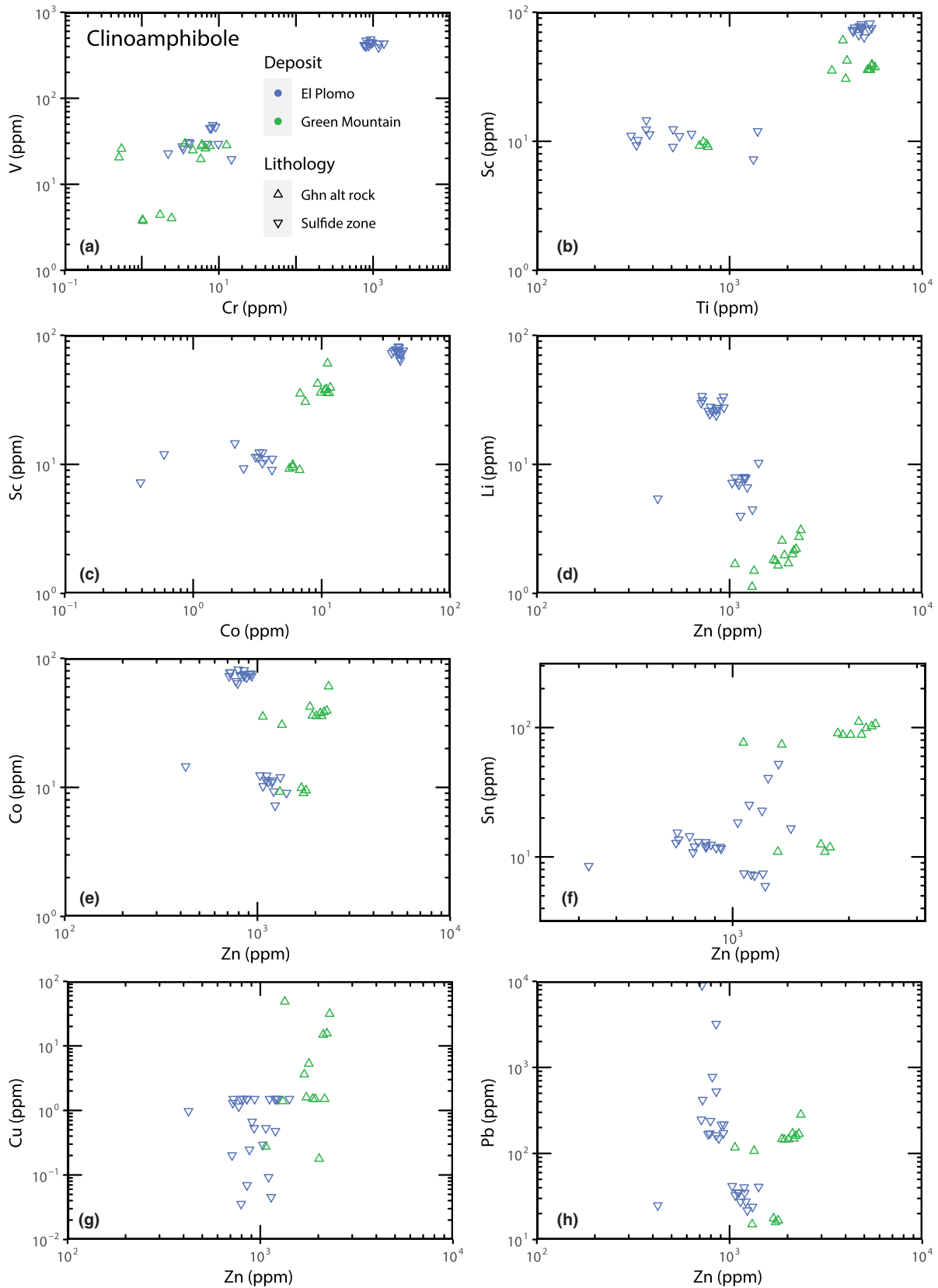


Figure 9. Bivariate trace-element plots (ppm) for clinoamphibole (hornblende, $n = 40$) from the El Plomo and Green Mountain deposits. (a) V vs Cr; (b) Sc vs Ti; (c) Sc vs Zn; (d) Li vs Zn; (e) Co vs Zn; (f) Sn vs Zn; (g) Cu vs Zn; and (h) Pb vs Zn.

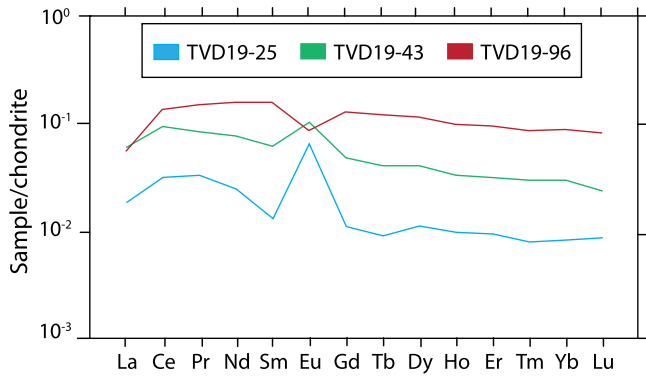


Figure 10. Chondrite-normalised rare earth element patterns of hornblende in the sulfide zone from El Plomo (samples TVD19-25 and TVD19-43) and a gahnite-bearing altered rock from Green Mountain (sample TVD19-96). Note the positive Eu anomaly for samples in the sulfide zone and the negative Eu anomaly for the sample in the gahnite-bearing altered rock. The REE data were normalised to chondrite values after McDonough and Sun (1995).

to 2546 ppm) and lower amounts of V (9.87 to 165.6 ppm) relative to ilmenite in gahnite-free, amphibole-bearing altered rocks (Mg = 515.7 to 2191 ppm, Cu = 5.40 to 29.6 ppm, Nb = 137.4 to 445.4 ppm and V = 1389 to 4048 ppm). It is possible that the spinel has preferentially incorporated V and Cu (e.g. Pekov *et al.*, 2018) relative to ilmenite although spinels are notoriously deficient in Nb relative to ilmenite. It might be that the lower Mg contents of ilmenite in amphibole-bearing altered rocks is due to the preferential incorporation of Mg in amphibole rather than ilmenite.

Discrimination diagrams as an indicator of deposit type

Dupuis and Beaudoin (2011) suggested a plot of $Al/(Zn+Ca)$ vs $Cu/(Si+Ca)$ can be used to characterise the composition of magnetite in VMS deposits. However, recent studies by Bédard *et al.* (2022) showed that 82% of magnetite compositions from VMS deposits do not fit in the designated VMS field with most data falling in a region that either has lower $Cu/(Si+Ca)$ or higher $Al/(Zn+Ca)$ ratios. Field relationships suggest the deposits in Colorado are VMS deposits (Berke *et al.*, 2023). However, none of the compositions of magnetite from VMS deposits in Colorado fit in the VMS field of Dupuis and Beaudoin (2011) and, similar to those reported by Bédard *et al.* (2022), they also have lower $Cu/(Si+Ca)$ or higher $Al/(Zn+Ca)$ ratios (Fig. 12c). Singoyi *et al.* (2006) in a classification scheme to distinguish magnetite among skarn, VMS, Broken Hill-type (BHT) and IOCG deposits plotted Sn/Ga vs Al/Co . In a modification of the Singoyi *et al.* (2006) plot, Kamvong *et al.* (2007) added the range of compositions for magnetite in the PUT1 (Thailand) and Phu Kam (Paos) skarn-related porphyry Cu deposits. In this classification scheme, magnetite compositions from Colorado overlap those for VMS deposits but some data from Green Mountain also overlap the IOCG field whereas those from the Betty deposit primarily occur in the skarn field (Fig. 12e). The sedimentary exhalative (Sedex) field shown in Fig. 10d was not included in the plot of Kamvong *et al.* (2007) but is included here and derived from the composition of magnetite analysed by Pollock *et al.* (2018) and Tott *et al.* (2019) from metamorphosed Cu–Au and Pb–Zn–Ag–(Cu–Au) Sedex deposits in the Kanmantoo Group of South Australia. Like the plot of

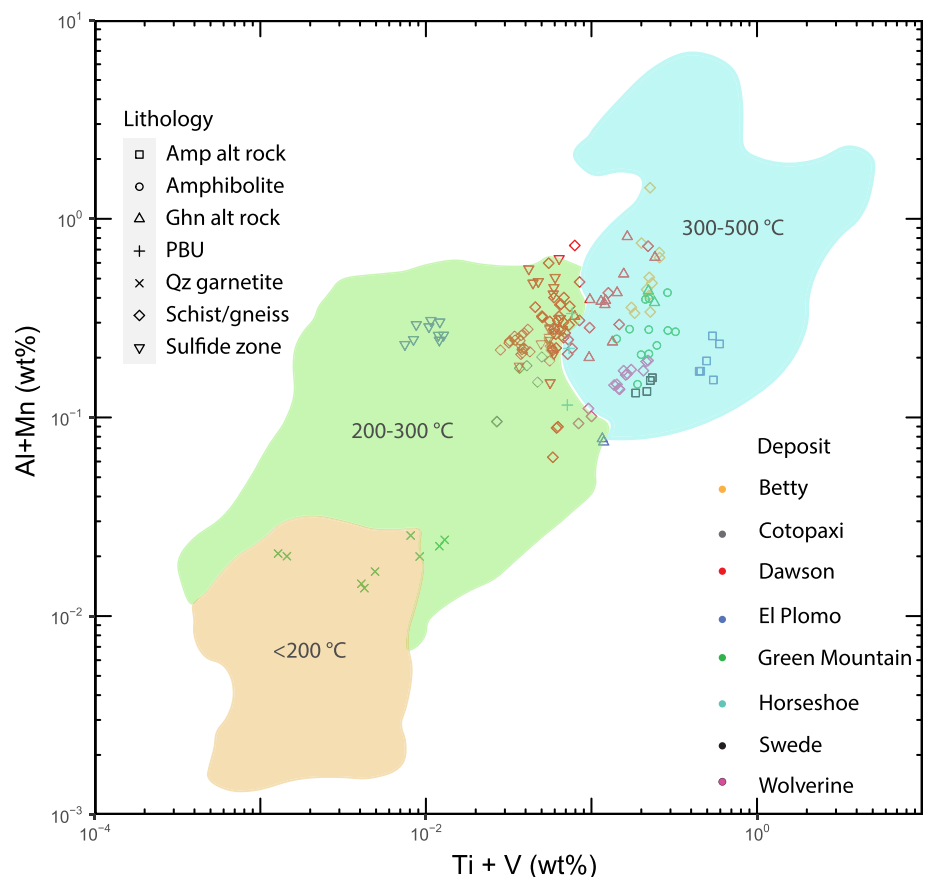


Figure 11. Plot of $Al + Mn$ vs $Ti + V$ for different formation temperatures of magnetite (modified after Nadoll *et al.* 2014; Maghfouri *et al.*, 2021).

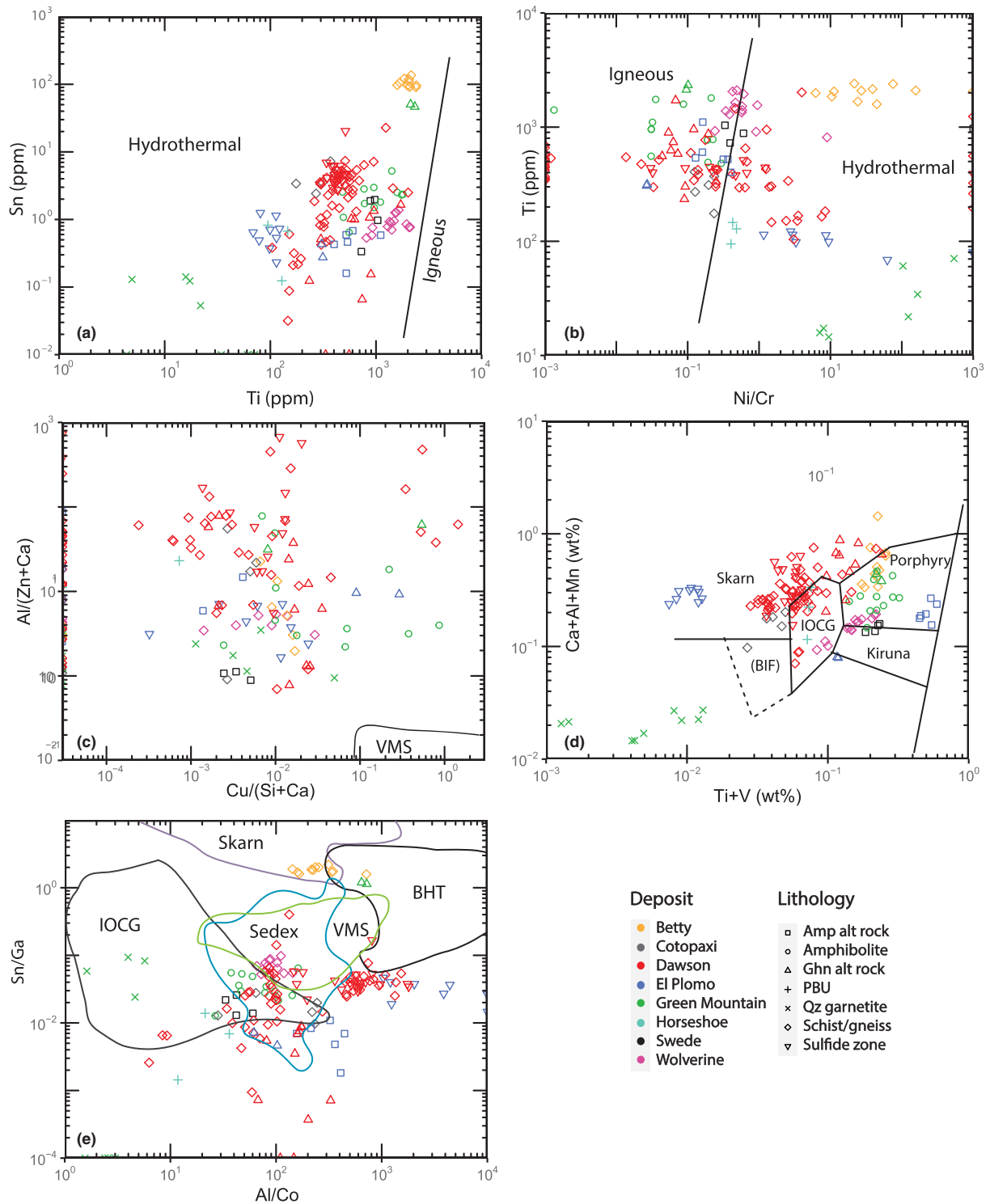


Figure 12. Discrimination diagrams for magnetite from the Colorado massive sulfide deposits (Betty, Cotopaxi, Dawson, El Plomo, Green Mountain, Horseshoe, Swede and Wolverine). (a) Sn vs Ti, which shows that compositions fall within the hydrothermal field (modified after Pisiak *et al.* (2015)). (b) Ti vs Ni/Cr, modified after Dare *et al.* (2014) showing magnetite compositions overlapping the hydrothermal and magmatic fields. (c) Plot of Al/(Zn+Ca) vs Cu/(Si+Ca) from Dupuis and Beaudoin (2011) showing the composition of magnetite from the VMS deposits from Colorado. The complete designated VMS field of Dupuis and Beaudoin (2011) is not shown here, which extends to Cu/(Si+Ca) values >1. No data from the Colorado deposits fit in the VMS field. (d) Discrimination diagram for magnetite from Colorado VMS deposits in terms of Ca+Al+Mn vs Ti+V. Fields for various deposit types (skarn, porphyry, iron oxide-copper-gold (IOCG), banded iron formation (BIF), and Kiruna-type Fe) are derived from Dupuis and Beaudoin (2011). Note that the compositions of magnetite from Colorado overlap the compositions for all the designated fields of the aforementioned ore types. (e) Compositions of magnetite from Colorado VMS deposits in terms of Sn/Ga vs Al/Co. Showing the IOCG, skarns, BHT and VMS fields of Singoyi *et al.* (2006) and a Sedex field derived from magnetite compositions reported by Tott *et al.* (2019) for magnetite in metamorphosed massive Pb–Zn–Ag–(Cu–Au) deposits in the Cambrian Kanmantoo Group, South Australia. Note the overlap between the Sedex and VMS fields.

Al/(Zn+Ca) vs Cu/(Si+Ca) (Fig. 12c), the plot of Sn/Ga vs Al/Co (Fig. 12e) is not a good discriminator of magnetite in VMS deposits relative to other ore deposit types. To further question the use of discrimination diagrams, a commonly used plot in the literature of Ca+Al+Mn vs Ti+V for magnetite compositions (e.g. Chen *et al.*, 2014; Mavrogenatos *et al.*, 2019; Frank *et al.*, 2022) developed by Dupuis and Beaudoin (2011) as an indicator of ore deposit type, shows the compositions of magnetite associated with VMS deposits in Colorado occur in the designated fields for skarn, porphyry, and iron oxide-copper-gold deposits (Fig. 12d).

Causes of compositional variations in magnetite

The VMS deposit sub-types studied by Makvandi *et al.* (2016a) included felsic–siliciclastic, mafic, bimodal mafic and bimodal felsic using the lithostratigraphic classification scheme of Franklin *et al.* (2005), which is based on the main volcanic and sedimentary lithological units associated with VMS deposits. Although recognising the variable and overlapping compositions of magnetite from the various deposit sub-types, Makvandi *et al.* (2016a) pointed out that the mean content of each trace-element data cluster is discriminated by a given chemical signature. For example, bimodal-felsic and bimodal-mafic deposits were characterised by magnetite with high Zn and low Ti and Al contents relative to that in other VMS subtypes. Furthermore, Makvandi *et al.* (2016a) suggested that the composition of magnetite in VMS deposits is related to the: oxygen fugacity; temperature and composition of the ore-forming magmatic/hydrothermal fluid; composition of the host rocks; and composition of minerals coexisting with magnetite.

On the basis of the stability of members in the system Cu–Fe–S–O and sulfur isotope compositions of sulfides, Berke *et al.* (2023) showed that the temperature and oxygen fugacity of the ore-forming fluids, the latter of which was buffered near the pyrite–pyrrhotite–magnetite triple point, were probably similar among the various deposits from Colorado. This suggests that these two parameters are not the main controls on the compositional variability of magnetite in metamorphosed altered rocks and in sulfide zones.

A major difference between the VMS deposits studied by Makvandi *et al.* (2016a) and those in this work is that the deposits in Colorado are considerably smaller in size (in terms of tonnage); in most cases, being at least an order of magnitude smaller. Particularly noteworthy of magnetite from Colorado is its variability in composition from one deposit to another (see Figs 5 and 11). This suggests that host-rock composition was a more important factor than temperature or oxygen fugacity given the variability of host-rock composition associated spatially with the deposits. For example, elements such as Cr, Ni and Cu are highest in the two igneous rocks (amphibolite and the pink banded unit) compared to magnetite in metamorphosed altered rocks. The hydrothermal fluid composition and the way it reacts with host rocks of different compositions will not only produce differences in the trace-element composition of magnetite but also marked variability in the major- and trace-element compositions of amphibole. The strong influence of bulk-rock composition on the composition of magnetite in metamorphosed massive sulfide deposits, for example, has been reported previously by Frank *et al.* (2019) for stratabound volcanic-associated, limestone skarn deposits (so-called SVALS-type deposits of Allen *et al.*, 1996) metamorphosed to the amphibolite facies in the Stollberg ore field, Sweden, and the strong influence of bulk-rock composition

on the composition of zincian spinels from the metamorphosed VMS deposits in Colorado has been reported by Heimann *et al.* (2005).

Magnetite coexists with several minerals (amphibole, cordierite, biotite, gahnite, garnet and sulfides) and there is no doubt that the trace-element contents of magnetite were, in part, controlled by the partitioning of these elements with these minerals. It is out of the scope of the present study to determine the relative effects of trace-element partitioning among these minerals. However, Zn concentrations are commonly elevated in magnetite relative to the other base metals, Cu and Pb, with the highest average Zn concentration in magnetite (1672 ppm) in sample 99CO-91 from the Betty deposit, where magnetite occurs in contact with Zn minerals (gahnite and sphalerite). The concentration of Zn in magnetite not in contact with other Zn-rich minerals is generally < 100 ppm.

Causes of compositional variation in amphibole

The double-chain amphibole supergroup is based on the general formula $AB_2C_5T_8O_{22}W_2$ where A = vacancy, Na, K, Ca, Pb and Li; C = Mg, Fe^{2+} , Mn^{2+} , Al, Fe^{3+} , Ti^{4+} and Li; T = Si, Al, Ti^{4+} and Be; and W = (OH), F, Cl and O^{2-} (Hawthorne *et al.*, 2012). Silicon and Al occur mostly in the tetrahedral (T) site, whereas Al, Fe, Mg, Mn, Zn and Ti are accommodated in the octahedral C sites. Trace elements including Rb, Ba and Pb occupy the A site, whereas REE and Y probably substitute for either Ca and/or Na in the A site (e.g. Shimizu *et al.*, 2017; Humphreys *et al.*, 2019). Although rare, Zn-rich and Cu-bearing amphiboles occur in nature (e.g. Klein and Ito, 1968; Chukanov *et al.*, 2020). Given the similar atomic ratios for Cu and Zn, it is possible that Cu also occurs in the C site. So the presence of elevated concentrations of base metals in amphiboles should not be considered unusual.

Amphibole in altered rocks and as gangue in massive sulfide zones in Colorado is undoubtedly metamorphic in origin, though hornblende in amphibolite from Green Mountain (which has a basaltic precursor, Berke *et al.*, 2023) had an igneous origin even though it was subsequently metamorphosed to the upper amphibolite facies. Although trace-element studies of amphibole in igneous rocks are relatively common in the literature (e.g. Marks *et al.*, 2004; Ye *et al.*, 2021), those in metamorphic rocks are generally lacking but include, for example, Bowes and Farrow (1997), Skublov and Drugova (2003) and Korinevsky *et al.* (2019). No previous study has been conducted on the trace-element composition of amphiboles associated spatially with metamorphosed massive sulfide deposits. Due to this limitation, comparisons with amphiboles from metamorphosed rocks are somewhat constrained. However, it should be noted that like the trace-element compositions of magnetite, those of orthoamphibole and clinoamphibole are also very variable between the different deposits in Colorado (Figs 7–9). Compared to gedrite in gedrite–cummingtonite–anthophyllite schists from the southern Urals analysed by Korinevsky *et al.* (2019), gedrite and anthophyllite analysed here from metamorphosed altered rocks in Colorado contain less Li, Sc, V, Cr (although gedrite and anthophyllite from El Plomo contains an order of magnitude higher amounts), Co, Sr and LREE. Similarly, the Cr (880 to 130 ppm) and Ni (100 to 125 ppm) contents of anthophyllite in metamorphosed mafic rocks consisting of anthophyllite and serpentine from Paakilla, Finland (Simonen, 1986; Bowes and Farrow, 1997) are considerably higher than in their counterparts from

Colorado. In contrast, samples of orthoamphiboles from Colorado contain considerably higher amounts of Zn (181 to 8440 ppm), in several cases an order of magnitude higher than those from Russia (110 ppm) and Finland (234 to 240 ppm). A single sample of anthophyllite from Paakilla contains < 5 ppm Pb, whereas anthophyllite and gedrite from the Colorado massive sulfide deposits contain up to 497 ppm Pb. Similarly, hornblende in the Colorado deposits contains almost an order of magnitude higher amounts of Zn than the clinoamphibole (tremolite, cummingtonite and actinolite) from the southern Urals but lower quantities of Sr and Rb. Most of the other trace elements in the Russian clin-oamphibole, including the REE, overlap with the compositions obtained here. Given that REE substitute for Ca, this is in keeping with the higher concentration of REE in hornblende in the samples analysed here from Colorado compared to that in the orthoamphibole.

Various physicochemical parameters affect the composition of amphibole in igneous rocks including fractional crystallisation (e.g. REE partition coefficients increase continuously), temperature, f_{O_2} and pressure (e.g. Iveson *et al.*, 2018; Nandedkar *et al.*, 2016). Experimental studies show that the major-element compositions of metamorphic amphibole are affected by a variety of factors including T , P , f_{O_2} , f_{S_2} , f_{H_2O} and f_{F_2} (e.g. Popp *et al.*, 1977a, 1977b; Schumacher, 2007). However, no experimental studies have been conducted on the trace elements in metamorphic amphibole that allow us to determine what parameters affect their compositions. Skublov and Drugova (2003) in a study of the trace elements of amphibole in gneisses metamorphosed from the amphibolite to granulite facies proposed that the REE content of calcic amphibole decreases from granulite facies (average = 194 ppm) to amphibolite facies (average = 34 ppm) and that trace-element composition is independent of pressure. However, in comparison, the average concentration of REEs in hornblende in rocks metamorphosed to the amphibolite facies from Colorado range from 53.5 ppm to 297.6 ppm suggesting that there are factors that affect composition other than temperature. Our investigations, like those of Skublov and Drugova (2003), show that the partitioning of trace elements between amphibole and coexisting minerals affects the composition of amphibole in metamorphic rocks of different compositions. Accordingly, it should be noted that hornblende in sulfide-rich rocks from the El Plomo prospect have positive Eu anomalies whereas that in the gahnite-bearing altered rocks from Green Mountain possesses a negative Eu anomaly (Fig. 10). It is possible that the positive Eu anomaly reflects more reducing conditions in the sulfide-bearing rocks and more oxidising conditions in the gahnite-bearing rock, the latter of which is probably more distal to a hydrothermal vent. Similar patterns were reported by Spry *et al.* (2007) for garnet in proximal and distal positions to the hydrothermal vent associated with the giant Broken Hill Pb–Zn–Ag deposit (Australia) that was metamorphosed to the granulite facies. Therefore, although bulk-rock composition and temperature are important parameters these might not be the most important ones. The same parameters that affect the major-element compositions also probably affect the trace-element compositions of amphibole. Clearly, experimental studies are required to assess further the physicochemical factors associated with trace-element compositions of metamorphic amphiboles.

Implications for exploration

Although magnetite is found in various rock types associated spatially with massive sulfide mineralisation in Colorado, its presence

alone does not necessarily constitute an exploration guide to ore. In contrast, orthoamphibole minerals (anthophyllite and gedrite) essentially occur in metamorphosed altered rocks associated spatially with sulfides as well as gangue in zones of massive sulfides. The presence of stratabound horizons of orthoamphibole–cordierite rocks alone, as exemplified by their occurrence at Evergreen (see Heimann *et al.*, 2006), constitutes a pathfinder horizon although further discrimination can be made on the basis of the trace-element compositions of magnetite and amphibole.

The distinctive PCA scores for magnetite and orthoamphibole (with $PCA1 > 0$ for Cu, Pb and Zn), and the elevated contents of zinc in orthoamphibole (up to 8840 ppm), hornblende (up to 1848 ppm), ilmenite (up to 3547 ppm), and magnetite (1627 ppm) in metamorphosed altered rocks and massive sulfides suggest that the Zn content of magnetite can potentially be used as a prospecting tool for sulfides in Colorado. Makvandi *et al.* (2016a) deduced that high Zn and low Al and Ti contents of magnetite can be used as exploration guides to bimodal-felsic and bimodal-mafic VMS deposits. Although magnetite in VMS deposits contain elevated concentrations of Co they also contain high amounts of Al (generally >1000 ppm) and low Ti contents (mostly <1000 ppm). Up to 8652 ppm and 1058 ppm Cu occur in orthoamphibole and ilmenite in samples from Colorado, suggesting that Cu can also be used as an exploration guide to ore. However, the Cu contents of magnetite and hornblende is generally low Cu (<60 ppm and 18 ppm, respectively) and appear to be a less useful pathfinders to sulfide mineralisation. The Pb contents of orthoamphibole, clinoamphibole, magnetite and ilmenite are highly variable, however, Pb should be analysed in these minerals when exploring for metamorphosed VMS deposits because they contain up to 3131 ppm, 775 ppm, 673 ppm and 7857 ppm Pb, respectively. Although elevated contents of V (up to 1842 ppm), Ni (369 ppm) and Cr (2092 ppm) occur in magnetite, they are generally higher in metamorphosed igneous intrusive rocks (pink banded unit and amphibolite). Furthermore, moderately high concentrations of Ga (up to 252 ppm) and Sn (105 ppm) in magnetite from metamorphosed altered rocks show some potential as guides to ore.

Conclusions

Field relations suggest massive sulfide deposits in Colorado are VMS deposits that formed by hydrothermal processes at, or below the seafloor, and were subsequently metamorphosed to the amphibolite facies. The trace-element contents of the alteration minerals most probably reflects the bulk composition of the rocks. Metamorphism was a closed system and the resulting metamorphic assemblages and their trace elements reflect the ore system.

Discrimination diagrams that have been used in the past to distinguish between ore deposit types, based on the $Al/(Zn+Ca)$ vs $Cu/(Si+Ca)$ and Sn/Ga vs Al/Co ratios of magnetite compositions, yield ambiguous results for the Colorado deposits because they cover a swath of ore fields and do not plot in the designated VMS field of previously published discriminant diagrams (i.e. Dupuis and Beaudoin, 2011). The range of trace-element compositions of magnetite reflects the variable nature of the host rocks among the different deposits and their small size suggesting that a high rock to hydrothermal fluid ratio was an important factor in producing this compositional variability. The variable nature of the host rock and the high rock to water ratios might also be the reason for the broad range of trace-element compositions of amphibole in the metamorphosed altered rocks.

Based on the concentrations of Al + Mn in magnetite when coupled with the Ti + V contents, the ore-bearing hydrothermal fluids probably formed at medium to high temperatures (~300° to 500°C). This is consistent with previous determinations of the ore fluid temperature of 270° to 350°C of Berke *et al.* (2023), based on the stability of members of the system Cu–Fe–S–O and sulfur isotope compositions of sulfides.

Although a plot of Ti vs Ni/Cr for magnetite compositions yields an ambiguous result concerning the magmatic versus hydrothermal nature of magnetite, a plot of the Sn vs Ti contents suggests that magnetite in metamorphosed altered rocks and the semi-massive to massive sulfides precipitated from a hydrothermal fluid. Magnetite in metamorphosed felsic (e.g. pink banded unit) and mafic (e.g. amphibolite) igneous rocks probably formed by magmatic processes.

The distinctive PCA scores for magnetite and orthoamphibole, and the elevated contents of Zn in gedrite, anthophyllite, hornblende, ilmenite and magnetite in metamorphosed altered rocks and massive sulfides suggest that the Zn content of these minerals may serve as an exploration guide to ore in Colorado. Other base metals, including Pb and Cu, also have potential as pathfinder elements given that concentrations of Cu in orthoamphibole and ilmenite and the Pb content of orthoamphibole, clinoamphibole, magnetite and ilmenite are invariably high. In addition, consideration should also be given to Al, Ga and Sn when analysing magnetite as concentrations of these elements can also be elevated.

Acknowledgements. This study was supported financially by Zephyr Minerals and by grants to EB from the Society of Economic Geologists Foundation and the Rocky Mountains Association of Geologists Foundation. Discussions with Will Felderhoff, Mark Graves and Loren Komperdo of Zephyr Minerals along with Trevor Van Dyke, Stan Keith and Monte Swan about the geology of the Dawson-El Plomo-Green Mountain deposits are greatly appreciated. The comments and constructive suggestions of two anonymous reviewers and Associate Editor, David Good, considerably improved the quality of the manuscript. Principal Editor, Roger Mitchell, is thanked for his patience during the delayed submission of the revised manuscript.

Supplementary material. The supplementary material for this article can be found at <https://doi.org/10.1180/mgm.2023.69>.

Competing interests. The authors declare none.

References

- Aiken J.L. (1981) *1981 Drilling Results Grape Creek Project, Fremont County Colorado*. Report to U.S. Borax Exploration, Boron, USA, 16 pp.
- Allen R.L., Lundström I., Ripa M., Simeonov A. and Christofferson H. (1996) Facies analysis of a 1.9 Ga, continental margin, back-arc, felsic caldera province with diverse Zn–Pb–Ag–(Cu–Au) sulfide and Fe oxide deposits, Bergslagen region, Sweden. *Economic Geology*, **91**, 979–1008.
- Anderson J.L. and Cullers R.L. (1999) Paleo- and Mesoproterozoic granite plutonism of Colorado and Wyoming. *Rocky Mountain Geology*, **34**, 149–164.
- Bédard É., De Bronac de Vazelhes V. and Beaudoin G. (2022) Performance of predictive supervised classification models of trace elements in exploration. *Journal of Geochemical Exploration*, **236**, 106959.
- Bennett V.C. and DePaolo D.J. (1987) Proterozoic crustal history of the western United States as determined by neodymium isotopic mapping. *Geological Society of America Bulletin*, **99**, 674–85.
- Berke E.H., Spry P.G., Heimann A., Teale G.S., Johnson B., Von der Handt A., Alers B and Shallow J.M. (2023) The genesis of metamorphosed Paleoproterozoic massive sulfide occurrences in central Colorado: geological, mineralogical and sulfur isotope constraints. *Geological Magazine*, <https://doi.org/10.1017/S0016756823000407>.
- Bickford M.E., Cullers R.L., Shuster R.D., Premo R.L. and Van Schmus W.R. (1989) U–Pb zircon geochronology of Proterozoic and Cambrian plutons in the Wet Mountains and southern Front Range. Pp 49–64 in: *Proterozoic Geology of the Southern Rocky Mountains* (J.A. Grambling and B.J. Tewksbury, editors). Geological Society of America Special Paper 235.
- Birch W.D., Burke E.A.J., Wall V.J. and Etheridge M.A. (1988) Eandrewsite, the zinc analogue of ilmenite, from Little Broken Hill, New South Wales, Australia, and the San Valentin Mine, Sierra de Cartagena, Spain. *Mineralogical Magazine*, **52**, 237–240.
- Bowes D.R. and Farrow C.M. (1997) Major and trace element compositions of the UICC standard asbestos samples. *American Journal of Industrial Medicine*, **32**, 592–594.
- Canil D., Grondahl C., Lacourse T., and Pisiak L.K. (2016) Trace elements in magnetite from porphyry Cu–Mo–Au deposits in British Columbia, Canada. *Ore Geology Reviews*, **72**, 1116–1128.
- Charlier B., Skår Ø., Korneliussen A., Duchesne, J.C. and Vander Auwera J. (2007) Ilmenite composition in the Tellnes Fe–Ti deposit, SW Norway: fractional crystallization, postcumulus evolution and ilmenite–zircon relation. *Contributions to Mineralogy and Petrology*, **154**, 119–134.
- Chen, W.T., Zhou, M.-F., Li, X., Gao, J.-F., Hou, K. (2014) In-situ LA-ICP-MS trace elemental analyses of magnetite: Cu–(Au, Fe) deposits in the Khetri copper belt in Rajasthan Province, NW India. *Ore Geology Reviews*, **65**, 929–939.
- Chukanov N.V., Zubkova N.V., Jančev S., Pekov I.V., Ermolaeva V.N., Varlamov D.A., Belakovskiy D.I. and Britvin A.N. (2020) Zinc-rich and copper-bearing amphiboles from sulfide-free ore occurrences of the Pelagonian Massif, Republic of North Macedonia. *Mineralogy and Petrology*, **114**, 129–140.
- Cooke D.R., Wilkinson J.J., Baker M., Agnew P., Phillips J., Chang Z., Chen H., Wilkinson C.C., Inglis S., Hollings P., Zhang L., Gemmill J.B., White N.C., Danyushevsky L. and Martin H. (2020) Using mineral chemistry to aid exploration: a case study from the Resolution porphyry Cu–Mo deposit, Arizona. *Economic Geology*, **115**, 813–840.
- Croghan C.W. and Egeghy P.P. (2003) *Methods of Dealing with Values Below the Limit of Detection Using SAS*. Southern SAS User Group, St. Petersburg, Florida, 22–24 September 2003.
- Dare S.A.S., Barnes S.-J. and Beaudoin G. (2012) Variation in trace element content of magnetite crystallized from a fractionating sulfide liquid, Sudbury, Canada: Implications for provenance discrimination. *Geochimica et Cosmochimica Acta*, **88**, 27–50.
- Dare S.A.S., Barnes S.-J., Beaudoin G., Méric J., Boutroy E. and Potvin-Doucet C. (2014) Trace elements in magnetite as petrogenetic indicators. *Mineralium Deposita*, **49**, 785–796.
- Davis J.C. (2002) *Statistics and Data Analysis in Geology*. 3rd ed. John Wiley & Sons, New York, 656 pp.
- Drobeck P.A. (1981) Proterozoic syngenetic massive sulfide deposits in the Gunnison gold belt, Colorado. Pp. 279–286 in: *Western Slope (Western Colorado)* (R.C. Epis and J.F. Callender, editors). New Mexico Geological Society 32nd Annual Fall Field Conference Guidebook.
- Duebendorfer E.M., Williams M.L. and Chamberlain K.R. (2015) Case for a temporally and spatially expanded Mazatzal orogeny. *Lithosphere*, **7**, 603–610.
- Dupuis C. and Beaudoin G. (2011) Discriminant diagrams for iron oxide trace element fingerprinting of mineral deposit types. *Mineralium Deposita*, **46**, 319–335.
- Ené V.V. (2014) *Major and Trace Element Geochemistry of Ilmenite Suites from the Kimberley Diamond Mines, South Africa*. MS thesis, University of Toronto, Canada
- Frank K.S., Spry P.G., Raat H., Allen R.L., Jansson N.F. and Ripa M. (2019) Variability in the geological, mineralogical, and geochemical characteristics of base metal sulfide deposits in the Stollberg ore field, Bergslagen, Sweden. *Economic Geology*, **114**, 473–511.
- Frank K.S., Spry P.G., O'Brien J.J., Koenig A., Allen R.L. and Jansson N.F. (2022) Magnetite as a provenance and exploration tool to metamorphosed base metal sulfide deposits in the Stollberg ore field, Bergslagen, Sweden. *Mineralogical Magazine*, **86**, 373–396.
- Franklin J.M., Gibson H.L., Jonasson I.R. and Galley A.G. (2005) Volcanogenic massive sulfide deposit. Pp. 523–560 in: *Economic Geology 100th Anniversary Volume 1905–2005* (J.W. Hedenquist, F.H. Thompson,

- R.J. Goldfar and J.P. Richards, editors). Economic Geology Publishing Company, Littleton, Colorado, USA.
- Ghosh B. and Praveen M.N. (2007) Garnet-gahnite-staurolite relations and occurrence of eandrewsite from the Koparpani base metal sulfide prospect, Betul Belt, Central India. *Neues Jahrbuch für Mineralogie Abhandlungen*, **184**, 105–116.
- Gion A.M., Piccoli P.M. and Candela P.A. (2022) Characterization of biotite and amphibole compositions in granites. *Contributions to Mineralogy and Petrology*, **177**, 43.
- Guillong M., Hametner K., Reusser E., Wilson S.A. and Günther D. (2005) Preliminary characterisation of new glass reference materials (GSA-1G, GSC-1G, GSD-1G and GSE-1G) by laser ablation-inductively coupled plasma-mass spectrometry using 193 nm, 213 nm and 266 nm wavelengths. *Geostandards and Geoanalytical Research*, **29**, 315–331.
- Hawthorne F.C., Oberti R., Harlow G.E., Maresch W.V., Martin R.F., Schumacher J.C. and Welch M.D. (2012) Nomenclature of the amphibole supergroup. *American Mineralogist*, **97**, 2031–2048.
- Hedge C.E. (1970) Whole-rock age of the Pikes Peak batholith, Colorado. *United States Geological Survey Professional Paper*, **700-B**, B86–B89.
- Heimann A. (2002) *Zinc-Rich Spinels Associated with Proterozoic Base Metal Sulfide Occurrences, Colorado, and their use as Guides to Metamorphosed Massive Sulfide Deposits*. MS thesis, Iowa State University, USA.
- Heimann A., Spry P.G. and Teale G.S. (2005) Zinc-rich spinels associated with Proterozoic base metal sulfide occurrences, Colorado, and their use as guides to metamorphosed massive sulfide deposits. *The Canadian Mineralogist*, **43**, 601–622.
- Heimann A., Spry P.G., Teale G.S. and Jacobson C.E. (2006) Coronas, symplectite textures, and reactions involving aluminous minerals in gedrite-cordierite gneisses from Evergreen, Front Range, Colorado. *The Canadian Mineralogist*, **44**, 1025–1044.
- Heinrich E.W.M. (1981) Precambrian tungsten and copper-zinc skarn deposits of south-central Colorado. *Colorado Geological Survey Resource Series*, **21**, 115 pp.
- Hu B., Zeng L.-P., Liao W., Wen G., Hu H., Li M.Y.H. and Zhao X.-F. (2022) The origin and discrimination of high-Ti magnetite in magmatic-hydrothermal systems: Insight from machine learning analysis. *Economic Geology*, **117**, 1613–1628.
- Humphreys M.C.S., Cooper G.F., Zhang J., Loewen M., Kent A.J.R., Macpherson C.G. and Davidson, J.P. (2019) Unravelling the complexity of magma plumbing at Mount St. Helens: a new trace element partitioning scheme for amphibole. *Contributions to Mineralogy and Petrology*, **174**, 1–15.
- Iverson A.A., Rowe M.C., Webster J.D. and Neill O.K. (2018). Amphibole-, clinopyroxene- and plagioclase-melt partitioning of trace and economic metals in halogen-bearing rhyodacitic melts. *Journal of Petrology*, **59**, 1579–1604.
- Jang Y.D. and Naslund H.R. (2003) Major and trace element variation in ilmenite in the Skaergaard Intrusion: petrologic implications. *Chemical Geology*, **193**, 109–125.
- Jia L.-H., Mao Q., Tian H.-C., Li L.-X., Qi L., Wu S.-T., Yuan J.-Y., Huan L.-L. and Chen Y. (2022) High-precision EPMA measurement of trace elements in ilmenite and reference material development. *Journal of Analytical Atomic Spectroscopy*, **37**, 2351–2361.
- Jochum K.P., Willbold M., Raczek I., Stoll B. and Herwig K. (2005) Chemical characterization of the USGS Reference Glasses GSA-1G, GSC-1G, GSD-1G, GSE-1G, BCR-2G, BHVO-2G and BIR-1G Using EPMA, ID-TIMS, ID-ICP-MS and LA-ICP-MS. 29. *Geostandards and Geoanalytical Research*, **29**, 285–302.
- Jochum K.P., Weis U., Stoll B., Kuzmin D., Qichao Y., Raczek I., Jacob D.E., Stracke A., Birbaum K., Frick D.A., Günther D. and Enzweiler J. (2011) Determination of reference values for NIST SRM 610–617 glasses following ISO guidelines. *Geostandards and Geoanalytical Research*, **35**, 397–429.
- Jolliffe I.T. and Cadima J. (2016) Principal component analysis: A review and recent developments. *Philosophical Transactions. Series A, Mathematical, Physical, and Engineering Sciences*, **374**, 20150202.
- Jones J.V. III, Siddoway C.S. and Connelly JN (2010) Characteristics and implications of ca.1.5 Ga deformation across a Proterozoic mid-crustal section, Wet Mountains, Colorado, USA. *Lithosphere*, **2**, 119–135.
- Kampmann T.C., Jansson N.F., Stephens M.B., Olin P.H., Gilbert S. and Wanhainen C. (2018) Syn-tectonic sulphide remobilization and trace element redistribution at the Falun pyritic Zn-Pb-Cu-(Au-Ag) sulphide deposit, Bergslagen, Sweden. *Ore Geology Reviews*, **96**, 48–71.
- Kamvong T., Zaw K. and Siegele R. (2007) PIXE/PIGE microanalysis of trace elements in hydrothermal magnetite and exploration significance: a pilot study. *15th Australian Conference on Nuclear and Complementary Techniques of Analysis and 9th Vacuum Society of Australia Congress*. University of Melbourne, Australia [Abstract].
- Karlstrom K.E., Åhäll K.-I., Harlan S.S., Williams M.L., McLelland J. and Geissman J.W. (2001) Long-lived (1.8–1.0 Ga) convergent orogen in southern Laurentia, its extensions to Australia and Baltica, and implications for refining Rodinia. *Precambrian Research*, **111**, 5–30.
- Klein C. and Ito J. (1968) Zincian and manganian amphiboles from Franklin, New Jersey. *American Mineralogist*, **53**, 1264–1275.
- Kleinhans L. and Swan M. (2022) Geological, geochemical, and geophysical characterization of gold in the Dawson peraluminous intrusive-related shear zone gold system, central Colorado. *Geological Society of America Abstracts with Program*, **54**, 219–13.
- Knipping J.L., Bilenker L.D., Simon A.C., Reich M., Barra F., Deditius A.P., Wälle M., Heinrich C.A., Holtz F. and Munizaga R. (2015) Trace elements in magnetite from massive iron oxide-apatite deposits indicate a combined formation by igneous and magmatic-hydrothermal processes. *Geochimica et Cosmochimica Acta*, **171**, 15–38.
- Korinevsky V.G., Filippova K.A., Kotlyarov V.A., Korinevsky E.V. and Artemyev D.A. (2019) Trace-elements in minerals from unusual rocks of the southern Urals. *Lithosphere*, **19**, 269–292.
- La Cruz N.L., Ovalle J.T., Simon A.C., Konecke B.A., Barra F., Reich M., Leisen M. and Childress T.M. (2020) The geochemistry of magnetite and apatite from the El Laco iron oxide-apatite deposit, Chile: Implications for ore genesis. *Economic Geology*, **115**, 1461–1491.
- Leake B.E. (1968) A catalog of analyzed calciferous and sub-calciferous amphiboles together with their nomenclature and associated minerals. *Geological Society of America Special Paper*, **68**, 1–44.
- Lindgren W. (1908) Notes on copper deposits in Chaffee, Fremont, and Jefferson Counties, Colorado. *U.S. Geological Survey Bulletin*, **691**, 57–174.
- Lindgren W. (1925) The cordierite-anthophyllite mineralization at Blue Hill, Maine, and its relation to similar occurrences. *Proceedings of the National Academy of Sciences*, **11**, 1–4.
- Maghfouri S., Mousivand F., Rastad E. and Lentz D.R. (2021) Chemical composition of magnetite and chlorite from the stringer zone of the Nuddeh volcanogenic massive sulfide (VMS) deposit, Iran: geological implications. *Mineralogy and Petrology*, **115**, 241–256.
- Magnani M.B., Miller K.C., Levander A. and Karlstrom K.E. (2004) The Yavapai-Mazatzal boundary: A long-lived element in the lithosphere of southwestern North America. *Geological Society of America Bulletin*, **116**, 1137–1142.
- Makvandi S., Beaudoin G., Ghasemzadeh-Barvarz M.G. and McClenaghan, B.M. (2013) Fingerprinting volcanogenic massive sulfide deposits using magnetite chemistry: Application to till from Izok Lake, Nunavut, Canada, in: *Mineral Deposit Research for a High-tech World*. Proceedings of the 12th Biennial Geology Applied to Mineral Deposits Meeting, 12–15 August, 2013, Uppsala, Sweden.
- Makvandi S., Ghasemzadeh-Barvarz M., Beaudoin G., Grunsky E.C., McClenaghan B.M. and Duchesne C. (2016a) Partial least squares-discriminant analysis of trace element compositions of magnetite from various VMS deposit subtypes: Application to mineral exploration. *Ore Geology Reviews*, **78**, 388–408.
- Makvandi S., Ghasemzadeh-Barvarz M., Beaudoin G., Grunsky E.C., McClenaghan B.M. and Duchesne C. (2016b) Principal component analysis of magnetite composition from volcanogenic massive sulfide deposits: Case studies from the Izok Lake (Nunavut, Canada) and Halfmile Lake (New Brunswick, Canada) deposits. *Ore Geology Reviews*, **72**, 60–85.
- Marks M., Halama R., Wenzel T. and Markl G. (2004) Trace element variations in clinopyroxene and amphibole from alkaline to peralkaline syenites and granites: implications for mineral-melt trace-element partitioning. *Chemical Geology*, **211**, 185–215.

- Mavrogenatos C., Voudouris P., Berndt J., Klemme S., Zaccarini F., Spry P.G., Melfos V., Tarantola A., Keith M., Klemm R. and Haase, K. (2019) Trace elements in magnetite from the Pagoni Rachi porphyry prospect, NE Greece: Implications for ore genesis and exploration. *Minerals*, **9**, 725, doi: 10.3390/min9120725.
- McCurdy M.W., Peter J.M., McClenaghan M.B., Gadd M.G., Layton-Matthews D., Leybourne M.I., Garrett R.G., Petts D.C., Jackson S.E. and Casselman S. (2022) Evaluation of magnetite as an indicator mineral for porphyry Cu exploration: a case study using bedrock and stream sediments at the Casino porphyry Cu–Au–Mo deposit, Yukon, Canada. *Geochemistry: Exploration, Environment, Analysis*, **22**, <https://doi.org/10.1144/geochem2021-072>
- McDonough W.F. and Sun S.-S. (1995) The composition of the Earth. *Chemical Geology*, **120**, 223–253.
- Moore R.O., Griffin W.L., Gurney J.J., Ryan C.G., Cousens D.R., Sie S.H. and Surer G.F. (1992) Trace element geochemistry of ilmenite megacrysts from the Monastery kimberlite, South Africa. *Lithos*, **29**, 1–18.
- Mulrooney D. and Rivers T. (2005) redistribution of the rare-earth elements among coexisting minerals in metamafic rocks across the epidote-out isograd: An example from the St. Anthony Complex, Newfoundland, Canada. *The Canadian Mineralogist*, **43**, 263–294.
- Nadoll P., Mauk J.L., Hayes T.S., Koenig A.E. and Box S.E. (2012) Geochemistry of magnetite from hydrothermal ore deposits and host rocks of the Mesoproterozoic Belt Supergroup, United States. *Economic Geology*, **107**, 1275–1292.
- Nadoll P., Angerer T., Mauk J.L., French D. and Walshe J. (2014) The chemistry of hydrothermal magnetite: A review. *Ore Geology Reviews*, **61**, 1–32.
- Nandedkar R.H., Hürlimann N., Ulmer P. and Müntener O. (2016) Amphibole–melt trace element partitioning of fractionating calc-alkaline magmas in the lower crust: an experimental study. *Contributions to Mineralogy and Petrology*, **171**, 71.
- Nielsen R.L., Forsythe L.M., Gallahan W.E. and Risk M.R. (1994) Major- and trace-element magnetite–melt equilibria. *Chemical Geology*, **117**, 167–191.
- O'Brien J.J., Spry P.G., Teale G.S., Jackson S.E. and Koenig A.E. (2015) Gahnite composition as a means to fingerprint metamorphosed base metal deposits. *Journal of Geochemical Exploration*, **159**, 48–61.
- Page P. and Barnes S.-J. (2009) Using trace elements in chromites to constrain the origin of podiform chromites in the Thetford Mines Ophiolite, Québec, Canada. *Economic Geology*, **104**, 997–1018.
- Paton C., Hellstrom J., Paul B., Woodhead J. and Hergt, J. (2011) Iolite: Freeware for the visualisation and processing of mass spectrometric data. *Journal of Analytical Atomic Spectrometry*, **26**, 2508.
- Pearce N.J., Perkins W.T., Westgate J.A., Gorton M.P., Jackson S.E., Neal C.R. and Cheney A.P. (1997) A compilation of new and published major and trace element data for NIST SRM 610 and NIST SRM 612 glass reference materials. *Geostandards and Geoanalytical Research*, **21**, 115–144.
- Pekov I.V., Sandalov F.D., Koshlyakova N.N., Vigasina M.F., Polekhovskiy Y.S., Britvin S.N., Sidorov E.G. and Turchkova A.G. (2018) Copper in natural oxide spinels: the new mineral thermaerogenite CuAl₂O₄, cuprospinel and Cu-enriched varieties of other spinel-group members from fumaroles of the Tolbachik Volcano, Kamchatka, Russia. *Minerals*, **8**, 498, <https://doi.org/10.3390/min8110498>.
- Pisiak L.K., Canil D., Grondahl C., Plouffe A., Ferbey T. and Anderson R.G. (2015) Magnetite as a porphyry copper indicator mineral in till: A test using the Mount Polley porphyry copper–gold deposit, south-central British Columbia (NTS 093A). *Geoscience BC Summary of Activities 2014*, **2015–1**, 141–150.
- Pollock M.V., Spry P.G., Tott K.A., Koenig A., Both R.A. and Ogierman J.A. (2018) The origin of the sediment-hosted Kanmantoo Cu–Au deposit, South Australia: Mineralogical considerations. *Ore Geology Reviews*, **95**, 94–117.
- Popp R.K., Gilbert, M.C. and Craig J.R. (1977a) Stability of amphibole with respect to oxygen fugacity. *American Mineralogist*, **62**, 1–12.
- Popp, R.K., Gilbert, M.C. and Craig, J.R. (1977b) Stability of amphibole with respect to sulfur fugacity. *American Mineralogist*, **62**, 13–30.
- Premo W.R. and Fanning C.M. (2000) SHRIMP U–Pb zircon ages for Big Creek gneiss, Wyoming and Boulder Creek batholith, Colorado: Implications for timing of Paleoproterozoic accretion of the northern Colorado province. *Rocky Mountain Geology*, **35**, 31–50.
- R Core Team (2019) *R: A language and environment for statistical computing*. R Foundation for Statistical Computing, Vienna, Austria, <https://www.R-project.org/>.
- Ririe G.T. (1981) *Precambrian Mineralization and Tectonic Framework of Fremont County, Colorado*. PhD dissertation, University of Iowa, USA.
- Salotti C.A. (1965) Mineralogy and paragenesis of the Cotopaxi, Colorado, Cu–Zn skarn deposit. *American Mineralogist*, **50**, 1179–1212.
- Schumacher J.C. (2007) Metamorphic amphiboles: composition and coexistence. Pp. 359–416 in: *Amphiboles: Crystal Chemistry, Occurrence, and Health Issues* (F.C. Hawthorne, R. Oberti, G. Della Ventura and A. Mottana, editors). Reviews in Mineralogy and Geochemistry, **67**. Mineralogical Society of America and the Geochemical Society, Chantilly, Virginia, USA.
- Shaw C.A. and Karlstrom KE (1999) The Yavapai–Mazatzal crustal boundary in the southern Rocky Mountains. *Rocky Mountain Geology*, **34**, 37–52.
- Sheridan D.M. and Raymond W.H. (1984) Precambrian deposits of zinc–copper–lead sulfides and zinc spinel (gahnite) in Colorado. *U.S. Geological Survey Bulletin*, **1550**, 31 pp.
- Sheridan D.M., Raymond W.H. and Cox L.J. (1981) Precambrian sulfide deposits in the Gunnison region, Colorado. Pp. 273–276 in: *Western Slope (Western Colorado)* (R.C. Epis and J.F. Callender, editors), New Mexico Geological Society 32nd Annual Fall Field Conference Guidebook.
- Shimizu K, Liang Y, Sun C. Jackson C.R.M. and Saal A.E. (2017) Parameterized lattice strain models for REE partitioning between amphibole and silicate melt. *American Mineralogist*, **102**, 2254–2267.
- Siddoway C.S., Givot R.M., Bodle C.D. and Heizler M.T. (2000) Dynamic versus anorogenic setting for Mesoproterozoic plutonism in the Wet Mountains, Colorado: Does the interpretation depend on level of exposure? *Rocky Mountain Geology*, **35**, 91–111.
- Simonen A. (1986) Vivianite from Paakkila, Tuusniemi, Finland. *Bulletin of the Geological Society of Finland*, **58**, 271–175.
- Singoyi B., Danyushevsky L., Davidson G.J., Large R. and Zaw K. (2006) Determination of trace elements in magnetites from hydrothermal deposits using the LA ICP–MS technique. *Society of Economic Geologists Conference*, Keystone, Colorado, CD-ROM.
- Skublov S. and Drugova G. (2003) Patterns of trace element distribution in calcic amphiboles as a function of metamorphic grade. *The Canadian Mineralogist*, **41**, 383–392.
- Smith M.S., Dymek R.F. and Schneiderman J.S. (1992) Implications of trace element geochemistry for the origin of cordierite–orthoamphibole rocks from Orijärvi, Finland. *Journal of Geology*, **100**, 545–559.
- Spry P.G., Peters J. and Slack J.F. (2000) Meta-exhalites as exploration guides to metamorphosed ore. *Reviews in Economic Geology*, **11**, 163–201.
- Spry P.G., Heimann A., Messerly J. and Houk R.S. (2007) Discrimination of metamorphic and metasomatic processes at the Broken Hill Pb–Zn–Ag deposit, Australia: Rare earth element signatures of garnet-rich rocks. *Economic Geology*, **102**, 471–494.
- Spry P.G., McFadden S., Teale G.S., Alers B., Shallow J.M., and Glenn J.M. (2022) Nodular sillimanite rocks as field indicators to metamorphosed massive sulfide deposits. *Ore Geology Reviews*, **141**, 104632.
- Sun C., Yang X., Zhang H., Ji W. and Xi D. (2022) Tracing the formation and modification of the Keketale VMS-type Pb–Zn deposit, Altai Mountains: Insights from ore deposit geology, geochronology, and magnetite geochemistry. *Ore Geology Reviews*, **1044**, 104852.
- Tott K.A., Spry P.G., Pollock M.V., Koenig A., Both R.A. and Ogierman J.A. (2019) Ferromagnesian silicates and oxides as vectors to metamorphosed sediment-hosted Pb–Zn–Ag–(Cu–Au) deposits in the Cambrian Kanmantoo Group, South Australia. *Journal of Geochemical Exploration*, **200**, 112–138.
- Treloar P.J., Koistinen T.J. and Bowes D.R. (1981) Metamorphic development of cordierite–amphibole rocks and mica schists in the vicinity of the Outokumpu ore deposit, Finland. *Earth and Environmental Science Transactions of the Royal Society of Edinburgh*, **72**, 201–215.

- Upadhyay H.D. and Smitheringale W.G. (1972) Geology of the Gullbridge copper deposit, Newfoundland: Volcanogenic sulfides in cordierite-anthophyllite rocks. *Canadian Journal of Earth Sciences*, **9**, 161–173.
- Van Der Boogaart K.G. and Tolosana-Delgado R. (2006) Compositional data analysis with ‘R’ and the package ‘compositions’. Pp 118–127 in: *Compositional Data Analysis in the Geosciences: From Theory to Practice*. (A. Buccianti, G. Mateu-Figueras and V. Pawlowsky-Glahn, editors) *Geological Society, London, Special Publications*, **264**.
- Verlagnet A., Brunet F., Goffé B. and Murphy W.M. (2006) Experimental study and modeling of fluid reaction paths in the quartz–kyanite±muscovite–water system at 0.7 GPa in the 350–550 °C range: implications for Al selective transfer during metamorphism. *Geochimica et Cosmochimica Acta*, **70**, 1772–1788.
- Wagner C., Villeneuve J., Boudouma O., Rividi N., Orberger B., Nabatian G., Honarmand M. and Monsef I. (2023) In situ trace element and Fe-O isotope studies on magnetite of the iron-oxide ores from the Takab region, north western Iran: Implications for ore genesis. *Minerals*, **13**, 774, <https://doi.org/10.3390/min13060774>.
- Warr L. (2021) IMA–CNMNC approved mineral symbols. *Mineralogical Magazine*, **85**, 291–320.
- Wen G., Li J.-W., Hofstra A.H., Koenig A.E., Lowers H.A. and Adams D. (2017) Hydrothermal reequilibration of igneous magnetite in altered granitic plutons and its implications for magnetite classification schemes: Insights from the Handan-Xingtai iron district, North China Craton. *Geochimica et Cosmochimica Acta*, **213**, 255–270.
- Wolter H.U. and Seifert F. (1984) Mineralogy and genesis of cordierite-anthophyllite rocks from the sulfide deposit of Falun, Sweden. *Lithos*, **17**, 147–152.
- Ye C., Feng Y., Lei R. and Yang G. (2021) Compositional variation of amphiboles during magma mixing: A case study of Huangyangshan A-type granite in Kalamaili metallogenic belt, East Junggar, China. *Frontiers in Earth Science*, **9**, 650014, doi: 10.3389/feart.2021.650014.